PEG (POLYETHYLENE GLYCOL)-PCL (POLYCAPROLACTONE) BLOCK COPOLYMERS FOR 3D PRINTING OF MEDICAL DEVICES

A Dissertation
Presented to
The Academic Faculty

by

Ruyi Yang

In Partial Fulfillment
of the Requirements for the Degree
Master of Science in the
School of Chemistry and Biochemistry

Georgia Institute of Technology
May 2022

PEG (POLYETHYLENE GLYCOL)-PCL (POLYCAPROLACTONE) BLOCK COPOLYMERS FOR 3D PRINTING OF MEDICAL DEVICES

Approved by:

Dr. M.G. Finn, Advisor
School of Chemistry and Biochemistry
Georgia Institute of Technology

Dr. Scott Hollister, Co-advisor
The Wallace H. Coulter Department of Biomedical Engineering
Georgia Institute of Technology

Dr. Will Gutekunst
School of Chemistry and Biochemistry
Georgia Institute of Technology

Date Approved: January 14th, 2022

ACKNOWLEDGEMENTS

This dissertation would not be completed without the help of several people (and a dog) throughout my time at Georgia Tech.

I want to start by thanking my advisor, Dr. M.G. Finn. His encouragement during the highs and his support during the lows helped me to become a better researcher. His advising style harnessed the best out of me. His time and effort for this project was invaluable. Discussions with him shaped my thinking and made me who I am today. His kindness extends beyond the world of science; he is an extremely humble and a nice person. His passion for science is unmatched and inspirational. Most importantly, it was fun to work with him!

I was lucky enough to have an equally important support system in the form of my co-advisor, Dr. Scott Hollister. My project, which combined several disciplines of science and engineering, required expertise on a variety of topics. I am grateful to have stimulating discussions with an expert in Biomedical Science and Engineering. His support was extremely crucial to take this project outside the chemistry lab.

I also want to thank Dr. Will Gutekunst who, as my committee member, provided clear feedback that helped me improve myself in various fronts of research and personal soft skills.

A big thank you to Sue Winters and Michelle Yager for taking care of the boring bits: Georgia Tech bureaucracies and ‘group biz’, which allowed me to have a razor-sharp focus on research.

I want to thank all the wonderful members in the Finn Lab past and present. I made many amazing friends here. I want to thank Dr. Michael Baksh for teaching me how to handle mammalian cells without killing them and then kill them. I want to thank Robert Hincapie and Jeff Noble for teaching me to do the same with bacterial cells. Any biology would be impossible without their helpful inputs. I want to thank my chemistry mentors, Dr. Zhishuai Geng and Dr. Mei-Kwan Yao. They taught me how to synthesize and characterize polymers. I want to thank Dr. Nicholas Bruno for helping me during a tough time and having fantastic discussions within and beyond science. I want to thank all the other members of the Finn lab from the ebb camp: Dr. Soumen Das, Dr. Kasie Colins, Parisa Keshavarz-Joud, Sonia Bhattacharya, Megan Andrews, Dr. Asheley Chapman; and the MoSE side: Dr. Breanne Hamlett, Jessica Lloyd, Erin Whetzel, Dr. Lucrezia De Pascalis, Dr. Kirstie Thompson, Dr. Ananda Podilapu, Dr. Binoy Maiti, Dr. Ankana Roy, Valentino Perez, Wenting Shi, and Devashish Sood. They were incredibly helpful and kind. Their presence made every day work a delightful experience, which was even better on Thursday's because of the gracious presence of Scout Finn!

I want to thank members of the Hollister lab: Ryan Ackman and Adam Verga for training me on engineering instruments, Dr. Jeonghyun Park for teaching me 3D printing, Dr. Harsha Ramaraju, Sarah Jo, and Nettie Brown for thought-provoking discussions and recommending some great places to eat in Atlanta Midtown! I am also grateful to Maya Jaffe for her helping hand.

I am deeply indebted to my parents. From encouraging me to chase my dreams in one of the top institutes to unconditional love and support during tough times, I always know they have my back. Knowing they believe in me helped me to overcome many tough

obstacles. A big thank you to my mom for listening to my endless complaints after a tough day and my dad for his unwavering optimism.

TABLE OF CONTENTS

LIST OF TABLES

LIST OF FIGURES

LIST OF SYMBOLS AND ABBREVIATIONS

PEG	polyethylene glycol
mPEG	poly (ethylene glycol) monomethyl ether
PCL	polycaprolactone
DCM	dichloromethane
MeOH	methanol
MW	molecular weight
PBS	phosphate buffered saline
Wt%	weight percent
E. coli	*Escherichia coli*
DSC	differential scanning calorimetry
GPC	gel permeation chromatography
TGA	thermogravimetric analysis
SEM	scanning electron microscopy
NMR	nuclear magnetic resonance
FBS	Fetal Bovine Serum
DMEM	Dulbecco's Modified Eagle Medium
P/S	penicillin-streptomycin
Gmax	glutaMAX
NaPyr	sodium pyruvate
AB	alamar blue
MHB	Mueller-Hinton Broth
ASTM	the International Committee of the American Society for Testing and Materials

MRI	Magnetic resonance imaging
CT	Computed tomography
X-ray	X-radiation
FDA	The United States Food and Drug Administration
Đ	dispersity
$CDCl_3$	deuterated chloroform
CL	caprolactone

SUMMARY

PCL polymers have been widely used in 3D printing of scaffolds over the past few decades, which can be applied in a variety of medical devices. However, PCL has intrinsic defects, such as high hydrophilicity which causes low biocompatibility. The research reported in this thesis aims to modify existing PCL polymers by developing a series of PEG-PCL block copolymers with different ratios of blocks and investigate their potential as implants for soft tissue engineering and airway reconstruction. The introduction of PEG blocks to PCL enhanced biocompatibility towards mammalian cells compared to the commercially available PCL with same molecular weight, without compromising the 3D printability. Moreover, some PEG-PCL copolymers showed significantly better resistance towards bacterial adhesion, which is desirable for both applications. The various mechanical properties of these copolymers make them promising candidates to devise patient-specific medical devices with various needs.

CHAPTER 1. INTRODUCTION

1.1 General introduction of 3D printing

3D printing, also known as additive fabrication or additive manufacturing, is always integrated with computer-aided design (CAD) to make solid objects with various designs by building up 2D patterns in layers. [1, 2] A technology known as stereolithography (SLA) is the first 3D printing process developed by Charles Hull in 1986, after which more technologies such as inkjet printing and extrusion printing have been developed.[3] Compared to other technologies, 3D printing allows manufacturing of individually designed complex structures with high precision control, which are also highly reproducible and repeatable.[4] The high flexibility in personal customization and design, with minimized material usage at the same time, makes 3D printing widely used in different areas such as construction, decorations, dentistry,[5] membrane separation,[6] robotics manufacture[7], electrical devices[8], and biomedical implants.[9]

To meet the increasing printing demands, various 3D printing methods like inkjet printing, selective laser sintering (SLS), and selective laser melting (SLM) have been developed. According to the International Committee of the American Society for Testing and Materials (ASTM), 3D printing processes can be classified into seven categories, described below.[10]

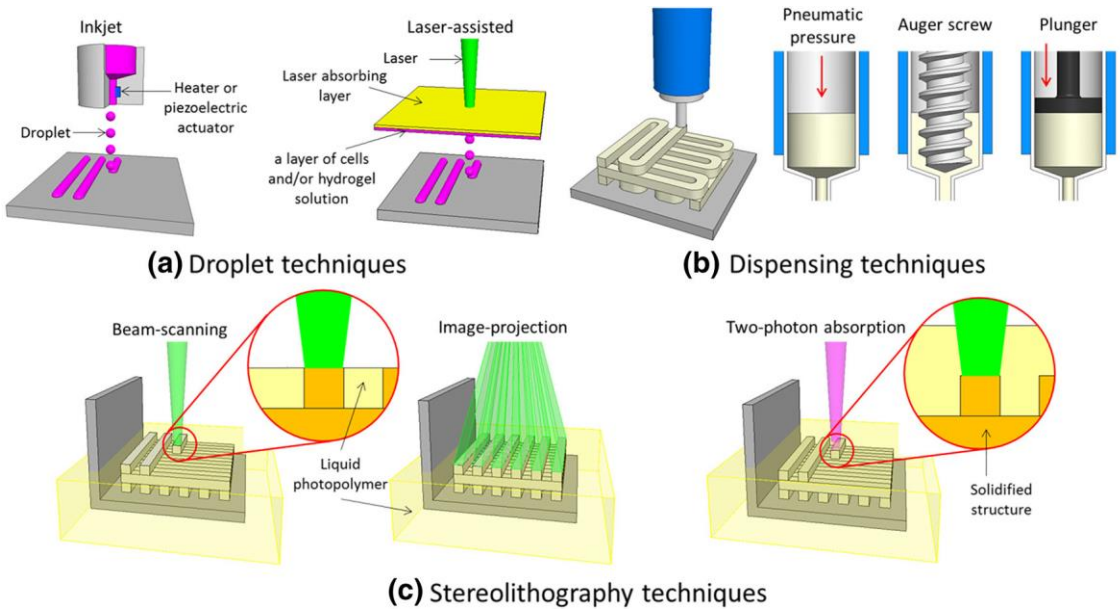

Figure 1 – Some examples of 3D printing methods.[4]

1) Binder jetting was first developed in 1990s at MIT.[11] It selectively deposits liquid bonding agents to powdered materials through multiple nozzles. After one layer of powder bonds together, another layer of powder will be spread on the top and then the bonding process is repeated. Binder jetting process doesn't involve heat or fusion, which enables printing various materials at room temperature and room atmosphere.[12]
2) Direct energy deposition (DED) utilizes energy to melt the powder- or wire-based raw materials to produce a melt pool. More materials are then injected this area to generate 3D structures. Based on the energy used, it can be divided into laser based DED, electron-beam based DED, plasma based DED, etc. An interesting application of this process is to print metals and metal-alloy systems to build or repair structures.[13]

3) Material jetting, also known as inkjet printing, is a liquid based printing method that offers adaptability towards different types of materials such as photocurable polymers and ceramics (Figure 1a). During the printing process, these materials are suspended in solution at first, and then deposited onto the designed location by the printing heads via thermal or piezoelectrical drop-on-demand devices. Post deposition, these materials are solidified using some resource such as UV radiation or laser sintering.[1] This method is rapid and has high resolution when printing complex structures; hence, it has been widely used in tissue engineering applications.
4) Powder bed fusion process uses laser or electron beams to fuse powder material together. After one layer is solidified, subsequent thin layer of powders are rolled for printing the following layer until the designed 3D structure is obtained.[14]
5) Sheet lamination is a process that uses thermal energy such as laser, electron beam, and plasma to melt a sheet-based material to make a part of the entire complex 3D structure.[10]
6) Stereolithographic printing is one of the vat photopolymerization processes (Figure 1c). Photosensitive polymer resin is initiated by ultraviolet (UV) light with precise location control and then allowed to solidify. The cured layer is lowered and another layer of resin will be well spread on top of it until the 3D structure is achieved. Post printing, the uncured resin is removed from the printed structure.[15]
7) Material extrusion is widely applied to make relatively small structures (Figure 1b). The thermoplastic raw material is heated inside the nozzle to a melt state, then extruded and solidified at room or lower temperatures. As a consequence, the

thermoplastic properties of the material such as melting temperature and the viscosities at certain temperatures become crucial and determine the difficulty level of the printing process. In this thesis, I used the extrusion method because it enables printing target structures without extensive material demand.[15]

Owing to the development of 3D printing processes within the last decade, increasing number of complex structures can be printed with higher resolution, shorter time frames, and reduced material usage, and therefore less waste and pollution to the environment. Consequently, 3D printing has been widely used in several different fields. One remarkable potential application is aerospace. 3D printing allows high resolution customized complex geometry, printing costly alloy materials with less waste and recovering the defected parts. Another promising application is biomedical engineering, as 3D printing can meet an increasing demand for patient-specific devices[16]

1.2 3D printing for biomedical engineering

Over the past two decades, 3D printing has been widely used in biomedical engineering to produce patient-specific biomedical products with lower cost, higher accuracy, and reproducibility. Some applications include tissue engineering, medical implants, drug delivery and, more recently, even combatting COVID-19.

1.2.1 Surgical planning

Complex technical tasks are common in surgery and necessitate a good surgical plan. Knowing how to combat possible problems during surgery may help surgeons increase the accuracy and efficiency, decrease the risk, and minimize operation time.[17]

Before the application of 3D printing in surgical planning, surgeons always planned operations based on the 2D medical images, obtained from MRI, CT, or X-ray, to determine the defected location. However, such images sometimes may miss some necessary details of the patients. In contrast, 3D printing can fabricate visualized patient-specific physical models with high fidelity and mimic living tissues by using different materials to provide more details of the defected anatomy.[18]

1.2.2 Medical implants and prostheses

As the demands for personalized implants and prostheses increase, the use of 3D printing technologies has trumped traditional technologies because of rapid fabrication of complex implant structures with high resolution and desired mechanical properties. These printed medical devices find several applications depending on clinical needs including dental implants, vascular stents and tracheal stents, cranium implants, orthopedic implants, limb prosthesis and so on. For reasons I will elaborate further in Chapter 3 of this thesis, I focused on solving current limitations with the end goal of making tracheal stents for airway reconstruction.[19]

There are three aspects we need to focus on for 3D printing of medical implants and protheses: development of biomaterials, tunable mechanical properties based on target tissues or body parts, and increasing biocompatibility while decreasing risk of infection during and post implantation.[20]

1.2.3 Pharmaceutical applications

3D printing is widely used in the pharmaceutical field for drug screening and drug delivery. By designing specific structures and carefully choosing materials, 3D printed drug delivery system may, potentially, mimic the *in vivo* environment. However, the applications are limited because of problems such as limited number of existing medical-grade printing materials and the relatively long fabrication period.[9]

1.2.4 Tissue engineering

The shortage of donor organs, following chronic rejection of transplants, and the needs for failed tissue and organ repair, are pressing medical needs that require immediate attention. As a consequence, tissue engineering approaches that use autologous biologic transplantation have gained significant attention during the last two decades.[21]

To generate new tissue, scaffolds with porous structures are fabricated to provide mechanical support and porosity for cells to adhere and proliferate. In contrast to traditional fabrication methods, 3D printing can ease the construction of complex patient-specific structures with precise and extensive control over micro- and macro- details. Thus, 3D printing in tissue engineering has been increasingly investigated and, in recent times, has become a hot topic for research and design.[22]

Prior to the development of 3D bioprinting, tissue engineering generally involved seeding of stem cells onto porous, preprinted scaffolds to form tissues, which is known as indirect cell assembly.[23] However, it is difficult to control the distribution of cells with this method, so the traditional strategy could not adequately mimic biological and mechanical

microenvironments.[24] Consequently, sensitive stem cells may show low viability, limited proliferation, and undesirable differentiation due to both physical and chemical factors of the microenvironment.[25] Compared to indirect cell assembly, 3D bioprinting utilizes printing ink (also known as bioink) that incorporates living cells inside materials that share similar features to the native extracellular matrix, which usually are hydrogels. This process offers a potential to address the limitations mentioned above by providing precise control of the distribution of cells, growth factors, and other bio-cues when printing bioink along with printing the scaffold, as bioinks alone are mechanically weak. [26] Hence, in 3D bioprinting, the printing process should permit the use of both stiffer scaffold material and low-modulus bioinks at the same time to control the distribution of the stem cells around scaffold. In addition, stem cells are sensitive to processing time and printing environment; therefore, incorporating cells and other bio-cues becomes challenging. For example, high printing temperatures and organic solvents influence protein folding resulting in inactive cells.[21]

In this thesis, we focused on for the development of synthetic biomaterials that can be used for indirect cell assembly method that provide adequate mechanical properties, resist bacterial infection, and support cell seeding for head and neck soft tissue engineering.

1.3 Common printable biomaterials

For 3D printing, various kinds of materials have been developed including wood, glass, ceramics, metals, concrete, polymers, etc. Considering of interactions between printed material and the *in vivo* bioenvironment, biomedical properties are as important as

good printability for the application of biomedical engineering. These properties include biocompatibility, chemical stability or biodegradability without toxic degradation products,[27] strong mechanical properties to withstand applied forces during implantation and *in vivo*, and resistance to infection.[28] Therefore, common biomaterials used in 3D printing for biomedical engineering applications include metals, polymers, ceramics, composites thereof [29, 30] Material choice depends on the target application. For example, metals such as titanium and its alloys are the best choices for orthopedic reconstruction currently because of their high modulus, strength, and resilience that promises longevity.[31] Among these biomaterials, polymers are commonly used to print medical devices such as biodegradable scaffolds for tissue engineering. The composites, relative molecular weight, degradation time of polymer materials can be precisely controlled, which gives them potential for good biocompatibility, degradability, and suitable mechanical properties.[32] Examples for such applications include synthetic polymers like polycaprolactone (PCL), polyethylene glycol (PEG), poly(lactic-co-glycolide) (PLGA) and Pluronic 127.[4]

For medical applications, PCL is a good candidate because of its high Young's modulus, strength, resistance to hydrolysis, appropriate flexibility and rigidity, ease of manufacturing, low cost, and ease of synthesis and modification. However, PCL has intrinsic defects for different applications in 3D printing of medical devices. In this thesis, we focused on the modification of PCL for enabling 3D printing of medical devices with desired properties, such as biocompatibility to mammalian cells.

1.4 Modification of polycaprolactone

As mentioned in Chapter 1.2, we are interested in airway reconstruction and craniofacial soft tissue engineering applications. Based on these applications, different properties are desired.

For the application in craniofacial soft tissue engineering, the indirect cell assembly method is preferred, which consists of printing porous PCL scaffolds and seeding cells directly onto these scaffolds. However, PCL is too hydrophobic for initial cell attachment, resulting in the retention of only a small amount of cells, thereby inhibiting subsequent proliferation.[33, 34] Increasing hydrophilicity by functionalizing PCL may help overcome these limitations and gain desirable properties. Two examples have appeared in the literature employing simple physical mixing of PCL with other materials. The Gunduz group used bacterial cellulose (BC), a naturally biodegradable material, that shares common features with extracellular matrix (ECM) components. These composite scaffolds exhibited enhanced biocompatibility and facilitated cellular proliferation.[35] The Bártolo group mixed PCL with varying low concentrations of pristine graphene, designed to improve solubility, processability, conductivity, and mechanical properties of the polymer materials. These low concentrations of pristine graphene exhibited no cytotoxicity and enhanced cell viability and proliferation.[33]

The published work closest to the current study is by the Hsieh group, who synthesized PCL-PEG-PCL copolymers with different molecular weights and then explored their printability. They used these copolymers to print scaffolds with different pore sizes and demonstrated their biocompatibility.[36, 37] The Hollister group has described a copolymer consisting of PCL and arginylglycylaspartic acid (RGD peptide), which is by far the most effective and often-employed peptide sequence for stimulating cell adhesion on synthetic

material surfaces. Its introduction promoted initial bone marrow stromal cells (BMSC) attachment, spreading, and focal adhesion formation.[38]

In airway reconstruction, patient-specific structures are required to be printed based on the images from CT or MRI. The implantation procedure or routine breathing may result in bacterial entry inside the airway and causing infection, as observed by our collaborators from University of Michigan, Ann Arbor. Thus, the introduction of antimicrobial function to PCL is necessary for this application. Also, as mentioned in Chapter 1.2, there is always a risk of infection in any implantation. Therefore, along with additional biocompatibility, 3D printed biomaterials for craniofacial soft tissues should also possess antimicrobial function. There are several ways to solve this problem: bactericidal function, bacterial resistance function, bacterial release function, which can be used individually or in combination.[39] One example of biocidal material is a cationic polymer, such as alkyl pyridinium or quaternary ammonium.[40] Our lab explored the antibacterial activity of thiabicyclononane-based materials, both in solution and surface, and some of them demonstrated high potency against four bacterial strains.[41] For bacterial resistance, the most commonly used materials are ethylene glycol (EG) based, such as poly(ethylene glycol) (PEG),[42] and zwitterion based, such as poly(sulfobetaine methacrylate) (PSBMA).[43]

Overall, this thesis focused on increasing the biocompatibility and introducing antimicrobial function to PCL polymer.

CHAPTER 2. SYNTHESIS AND CHARACTERIZATION OF PEG-PCL BLOCK COPOLYMERS

2.1 Introduction

As mentioned in Chapter 1, PCL possesses several properties that make it a good candidate for biomedical applications. It is relatively cheap and easy to modify chemically, physically, and mechanically. However, a common problem with such polymers is rampant growth of bacteria due to their hydrophobicity. In addition, the hydrophobicity also prevents mammalian cell attachment for the application of tissue engineering. Therefore, to increase hydrophilicity, polyethylene glycol (PEG) can be introduced to make PEG-PCL blends. Furthermore, the use of these materials in biomedical devices requires the PEG-PCL copolymers to be compatible for printing. In other words, the addition of PEG should not affect the printability of the PCL polymer. To achieve this, we need to consider three parameters: viscosity, melting temperature, and degradation temperature. Hsieh and coworkers showed several different molecular weight PCL-PEG-PCL copolymers that were 3D printable.[37] We decided to focus on PEG-PCL block copolymers with the same molecular weights but different proportions of hydrophobic and hydrophilic blocks in order to assess their printability and functional performance.

As a synthetic biomaterial, PEG polymers and its derivatives offer multiple advantages. PEG is nontoxic and immunocompatible, i.e., it does not cause any serious inflammation, and is therefore well suited for the use in materials for implantation. It is generally accepted that PEG resists bacteria because of hydration.[44, 45] In the presence of water, the PEG chains can form multiple hydrogen bond, thereby decorating the surface with water molecules. Proteins do not strongly adhere to such surfaces since the proteins are themselves surrounded by water, and so no strong driving force exist for them to

associate with the water-coated surface. Meanwhile, introduction of PEG to PCL has been shown to be non-toxic to mammalian fibroblasts and promotes their attachment.[36, 37]

PEG also offers several other advantages from an experimental standpoint: it is commercially available, cheap and its solubility in both organic solvents and water enables easier polymer processing. To test the performance of mPEG-PCL diblock and PCL-PEG-PCL triblock copolymers compared to pure PCL, we synthesized several groups with the same molecular weight of commercial pure PCL and different molecular weights of PEG chains.

2.2 Results

Macroinitiator mPEG or PEG, monomer caprolactone (CL) and the catalyst stannous octoate were added to a pre-dried Schlenk flask. After vacuum and filling with nitrogen three times at 80 ˚C, the flask was heated at 130 ˚C overnight, and the product was then precipitated out in diethyl ether and washed by methanol to get rid of mPEG or PEG and CL residues. The mPEG-PCL and PCL-PEG-PCL polymers were then characterized to figure out some properties and then compared to commercial PCL.

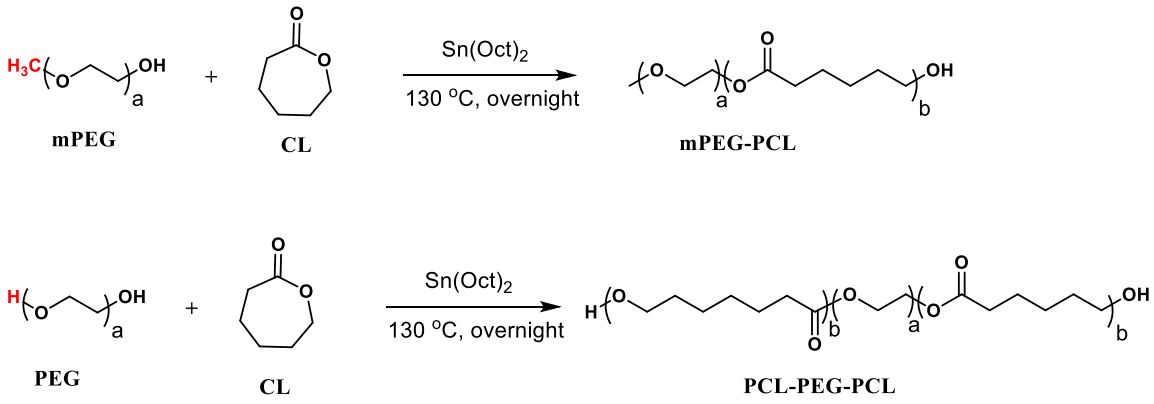

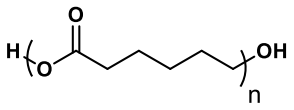

PCL

2.2.1 Molecular weights of PEG-PCL copolymers

The molecular weights for different polymers were determined using ^{1}H NMR and gel permeation chromatography (GPC). Table 1 summarizes the molecular weights (Mn), dispersity (Đ), and the amount of PEG relative to PCL for each block polymer. The molecular weight of commercial PCL polymer we obtained (for control studies) was 43k. Therefore, to allow direct comparison of results, we prepared block copolymers of the same size (between 41k and 45k molecular weight).

Table 1 – Representatives of block polymers characterized by ^{1}H NMR, GPC.

Group name	Polymer	Mn (kDa)[a]	Mn (kDa)[b]	Đ[b]	PEG: PCL (wt%)[a]
$mPEG_{5k}$	Commercial $mPEG_{5k}$	/	10	1.23	/
PCL	Commercial PCL_{43k}	/	50	1.71	/
di-2k	$mPEG_{2k}$-PCL	43	65	1.77	1:20.5
di-5k	$mPEG_{5k}$-PCL	43	53	1.51	1:7.6
di-10k	$mPEG_{10k}$-PCL	43	53	1.66	1:3.3
di-20k	$mPEG_{20k}$-PCL	43	48	1.42	1:1.2
tri-2k	PCL-PEG_{2k}-PCL	43	60	1.52	1:20.5
tri-6k	PCL-PEG_{6k}-PCL	43	58	1.46	1:6.2
tri-10k	PCL-PEG_{10k}-PCL	43	54	1.59	1:3.3
tri-20k	PCL-PEG_{20k}-PCL	43	46	1.48	1:1.2

(a) by ^{1}H NMR. (b) by GPC.

2.2.2 Contact angle of PEG-PCL copolymers

To determine the hydrophilicity, the water static contact angles of mPEG-PCL diblock and PCL-PEG-PCL triblock copolymers were measured. The contact angle decreases as hydrophilicity increases. As expected, compared to pure PCL with same molecular weight, both diblock and triblock polymers showed much smaller contact angles (Figure 2). The decrease in contact angle directly correlated with the amount of PEG in the final block polymers.

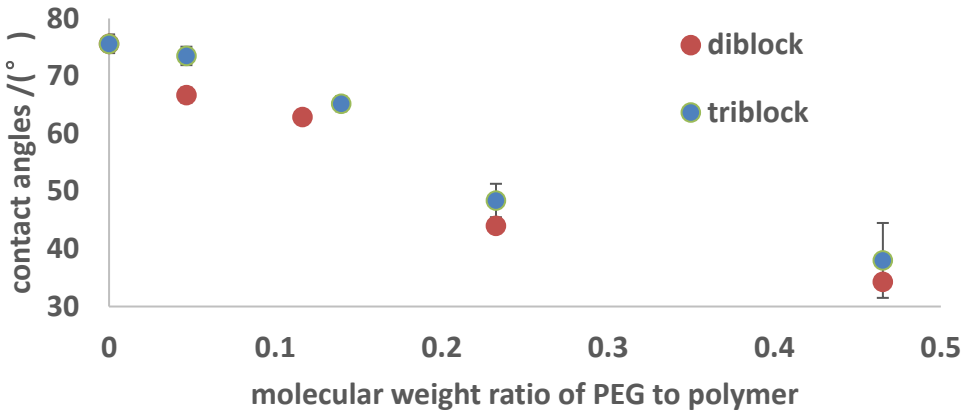

Figure 2 – The relationship between contact angles and the molecular weight ratio of PEG to polymer. From left to right are PCL, di-2k and tri-2k, di-5k and tri-6k, di-10k and tri-10k, di-20k and tri-20k.

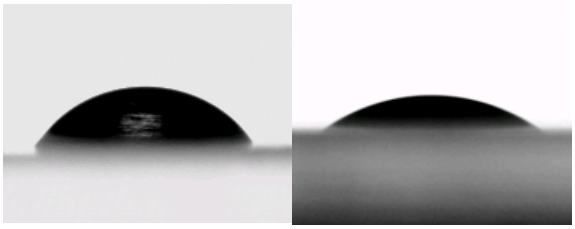

Figure 3 – Representative images from contact angle measurements. PCL contact angle being 75.6±1.6° (left) and mPEG$_{10k}$-PCL contact angle being 44.0±1.2° (right) are shown as representatives

2.2.3 Thermal properties of PEG-PCL copolymers

Since the extrusion method was chosen for bioprinting, the thermal properties of a candidate material are important: the melting temperature determines the lower limit of processing temperature, and the thermal degradation point defines the highest possible processing temperature. Degradation temperatures and melting temperatures were obtained by thermogravimetric analysis (TGA) and differential scanning calorimetry (DSC), respectively (Table 2). Relatively low melting temperatures (around 60 °C) and high degradation temperatures (around 300 °C) were observed, which were well suited to the desired operation range (room temperature to 200 °C) of the nozzle-based printing machine, 3D BIOPLOTTER.

Table 2 – Melting temperatures (T_m) and degradation temperatures of block polymers.

Polymer	Onset Temp of T_m (°C)[a]	Peak Temp of T_m (°C)[a]	End Temp of T_m (°C)[a]	5% weight loss Temp (°C)[b]
$mPEG_{2k}$-PCL	52	56	60	>200[c]
$mPEG_{5k}$-PCL	50	54	57	333
$mPEG_{10k}$-PCL	51	54	58	272
$mPEG_{20k}$-PCL	46	59	62	>200[c]
PCL-PEG_{2k}-PCL	49	56	60	320
PCL-PEG_{6k}-PCL	46	54	59	294
PCL-PEG_{10k}-PCL	43	52	57	>200[c]
PCL-PEG_{20k}-PCL	34	38	43	>200[c]

(a) by DSC. (b) by TGA. (c) because of the defect of TGA from STAMI, the precise results are not accessible.

2.2.4 Validating printability of PEG-PCL copolymers

The printability and associated printing parameters were determined using the 3D BIOPLOTTER. To get the desired standard strand width of 500 μm, the printing

parameters for PCL were 100 °C, 9 bar and 4.2 mm/s nozzle speed (with an inside nozzle diameter = 0.4 mm). However, we found that printing mPEG$_{5k}$-PCL required a lower nozzle speed 3.8 mm/s, with other conditions being same, to get the same strand width. For PCL-PEG$_{6k}$-PCL the corresponding printing parameters were 100 °C, 9 bar and 5.0 mm/s or 80 °C, 9 bar and 2.6 mm/s. These results indicate that mPEG$_{5k}$-PCL and PCL-PEG$_{6k}$-PCL have different viscosities than pure PCL with same molecular weight, which was further supported by rheometry shown below. The relatively lower viscosity makes the printing process quicker or printing parameters milder.

A more detailed exploration of line width vs. printing parameters for mPEG$_{5k}$-PCL is shown in Figure 4. Three different temperatures were tested, and the expected linear relationship between nozzle speed and line width was observed. A complete list of optimal print parameters for the block copolymers is shown in Table 3.

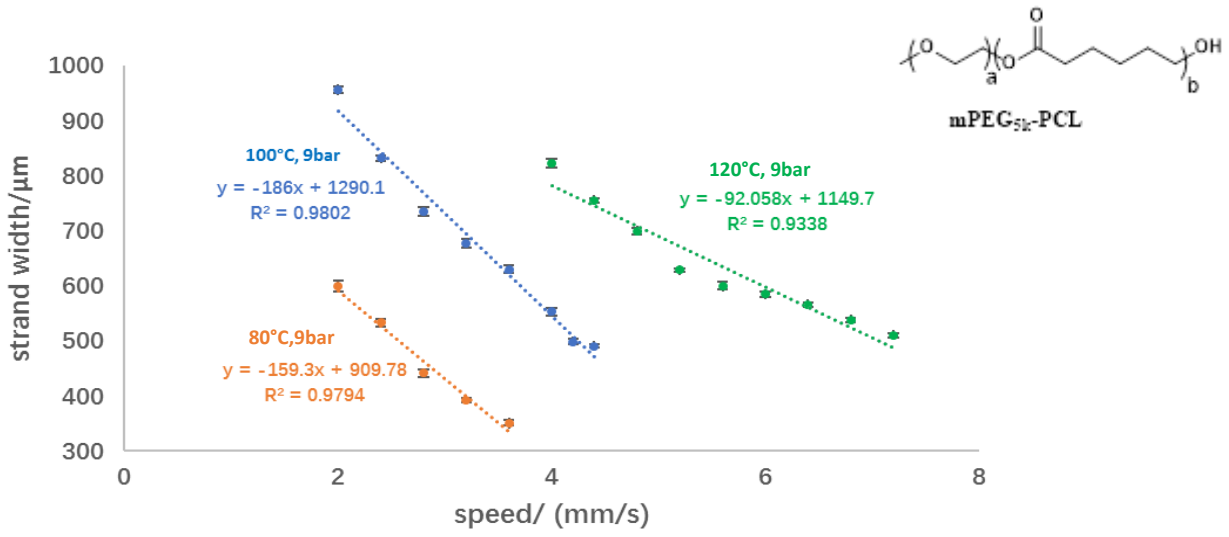

Figure 4 – Printing parameters of mPEG$_{5k}$-PCL.

2.2.5 Viscosity of PEG-PCL copolymers for 3D printability

The viscosities of these polymers were determined by rheometry (Anton Paar, model MCR302). Compared with pure PCL with same molecular weight, the block copolymers showed different viscosities which matched the results from the printability tests (Figure 6) and the data are shown in Table 3. The introduction of PEG was expected to influence crystallinity both because of its own properties and the correspondingly shorter PCL chain lengths.

Some unexpected variability in viscosities were also observed. For example, the viscosities of the materials before and after printing were often different, and different batches of printed materials also showed different viscosities, even when the raw materials had similar viscosities. The example of PCL-PEG_{10k}-PCL is shown in Figure 5. There are two possible causes for this problem: (1) polymer degradation during the long, high-temperature printing process, and/or (2) the printed materials have different crystallization ratio because of differences in solidification environments. We also observed that long-term storage changed viscosity, presumably because of slow polymer degradation at room temperature.

Table 3 – Optimal printing parameters.

Polymer	Temp (°C)	Pressure (bar)	Nozzle speed (mm/s)	Viscosity at 1 rad/s, 100 °C (Pa·s)
PCL	100	9	3.4	349.1 ± 7.2 Pa·s
$mPEG_{2k}$-PCL	120	9	2.6	1543.1 ± 133.4 Pa·s
$mPEG_{5k}$-PCL	100	9	3.8	813.5 ± 63.3 Pa·s
$mPEG_{10k}$-PCL	80	3	3.2	444.7 ± 5.1 Pa·s
$mPEG_{20k}$-PCL	80	1	1.6	86.8 ± 6.1 Pa·s
PCL-PEG_{2k}-PCL	120	9	4.6	282.3 ± 17.8 Pa·s
PCL-PEG_{6k}-PCL	80	9	2.6	418.6 ± 20.8 Pa·s

PCL-PEG$_{10k}$-PCL	80	5	5	434.8 ± 4.7 Pa·s
PCL-PEG$_{20k}$-PCL	80	1	4	175.7 ± 5.8 Pa·s

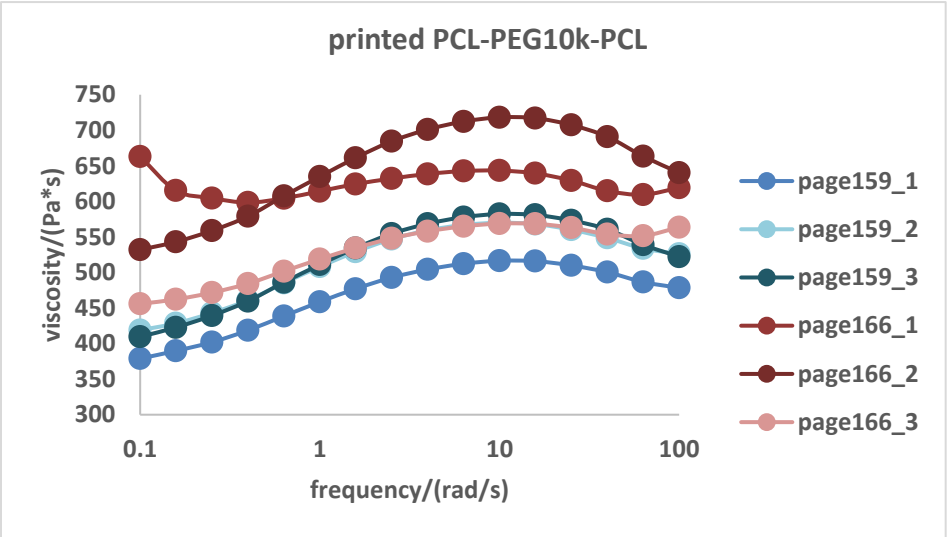

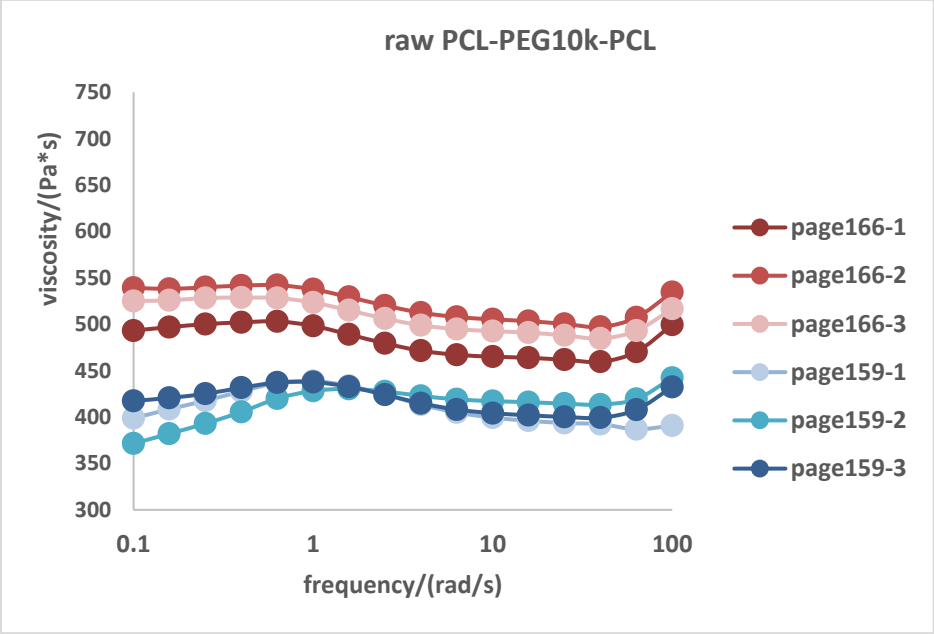

Figure 5 – Viscosities of PCL-PEG$_{10k}$-PCL from two different batches (page159 and page166), both printed and raw materials before printing. (Page159 results: GPC: Mn=60k, Mw=84k, PDI=1.41 NMR: MW=43.3k; Page166 results: GPC: Mn=53k, Mw=81k, PDI=1.54 NMR: MW=43.2k)

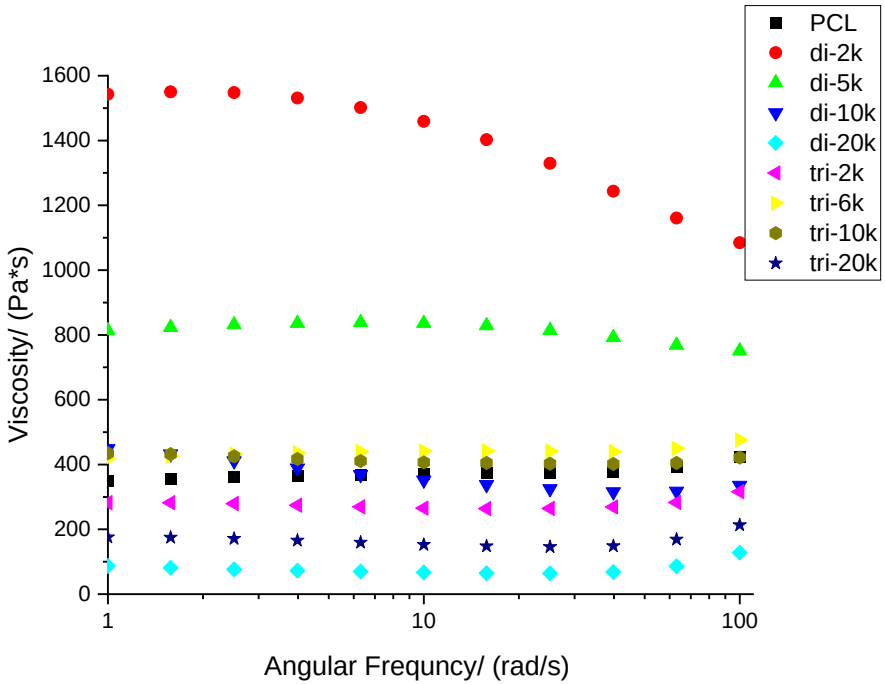

Figure 6 – Viscosities of raw materials.

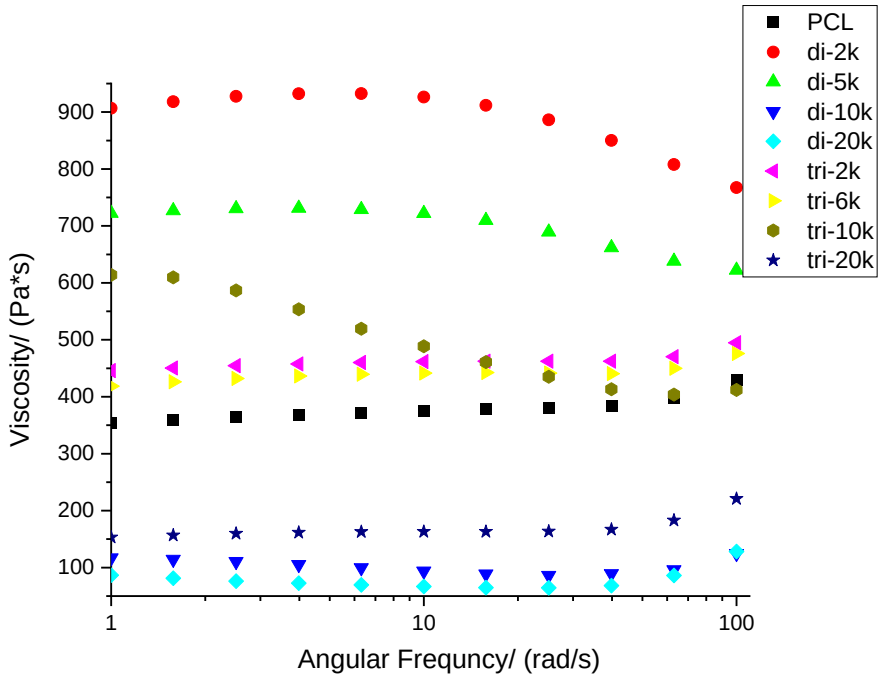

Figure 7 – An example of viscosities of printed materials.

2.3 Conclusion

mPEG-PCL diblock and PEG-PCL-PEG triblock copolymers were successfully synthesized. The molecular weights were confirmed using ^{1}H NMR and GPC. Our hypothesis that increasing the ratio of PEG to PCL would lead to greater hydrophilicity was verified using contact angle measurements. All block copolymers were determined to be printable based on standard tests, including melting temperature, degradation temperature, viscosity measurements, and direct printing with a 3D printer.

2.4 Experimental

2.4.1 Synthesis of PEG-PCL diblock copolymers

mPEG-PCL diblock copolymers were synthesized successfully with the macroinitiator mPEG, monomer caprolactone (CL) and the catalyst stannous octoate in 85% to 95% yield (Figure 8). The reactions were heated at 130˚C overnight, the product was precipitated out in diethyl ether and washed by methanol to get rid of mPEG and CL residues. Different molecular weights of mPEGs (Mn= 2k, 5k, 10k, 20k Da) were utilized in the synthesis of these block copolymers.

2.4.2 Synthesis of PEG-PCL triblock copolymers

PCL-PEG-PCL triblock copolymers were synthesized successfully with the macromolecule initiator PEG, monomer caprolactone (CL) and the catalyst stannous octoate in 85% to 95% yield (Figure 8). The reactions were heated at 130˚C overnight, the product was precipitated out in diethyl ether and washed by methanol to get rid of PEG

and CL residues. Different molecular weights of PEGs (Mn= 2k, 6k, 10k, 20k Da) were utilized in the synthesis of these block copolymers.

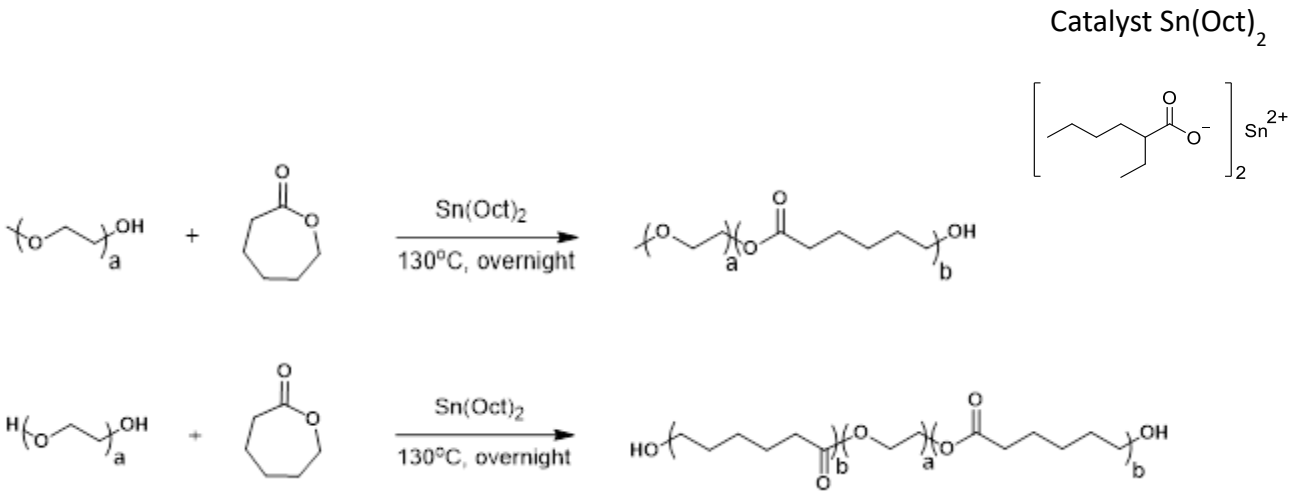

Figure 8 – Synthesis route of mPEG-PCL diblock, PCL-PEG-PCL triblock polymers.

2.4.3 Characterization of PEG-PCL block copolymer

2.4.3.1 Representative ^{1}H NMR Spectra

^{1}H NMR spectra were obtained using Brüker DRX-500 instruments in deuterated chloroform (Cambridge Isotope Laboratories, Inc.) and the spectra were processed in Mestre Nova software.

PEG-PCL-PEG triblock polymer: ^{1}H NMR (500 MHz, $CDCl_3$) δ 4.08 (t, *J* = 6.7 Hz, 2H), 3.66 (s, 4H), 2.33 (t, *J* = 7.5 Hz, 2H), 1.67 (m, 4H), 1.46 – 1.35 (m, 2H).

mPEG-PCL: ^{1}H NMR (500 MHz, CDCl3) δ 4.06 (t, J = 6.7 Hz, 2H), 3.64 (s, 4H), 2.30 (t, J = 7.5 Hz, 2H), 1.64 (m, 4H), 1.43 – 1.31 (m, 2H).

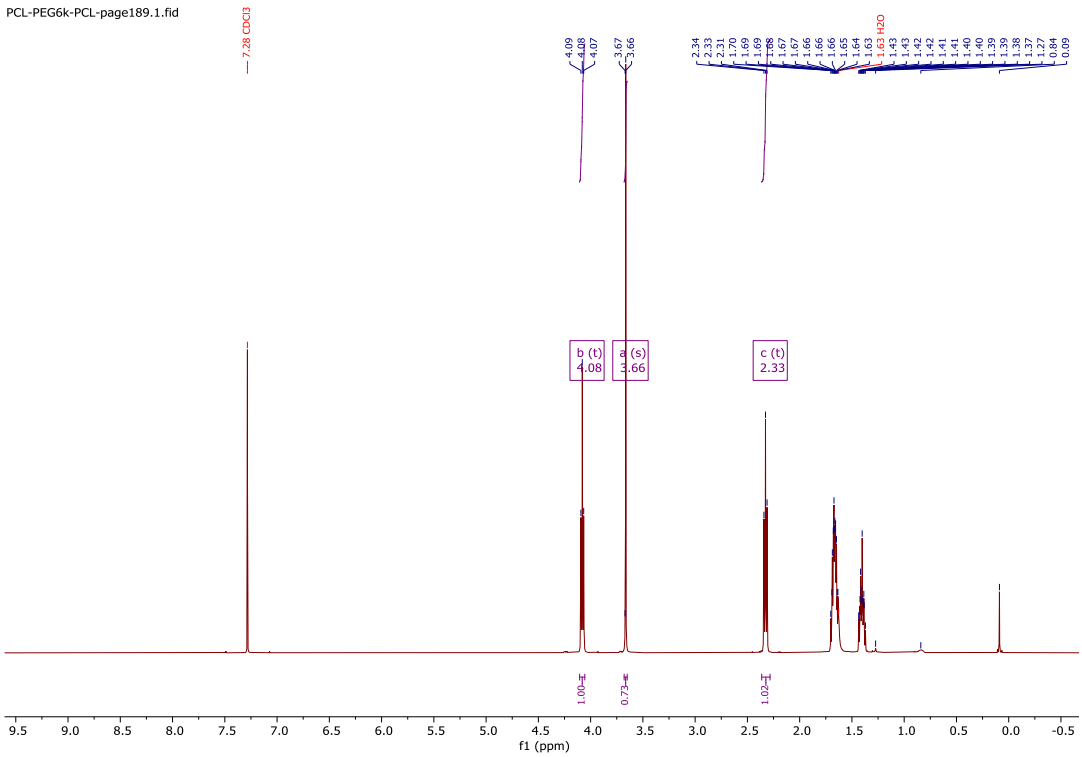

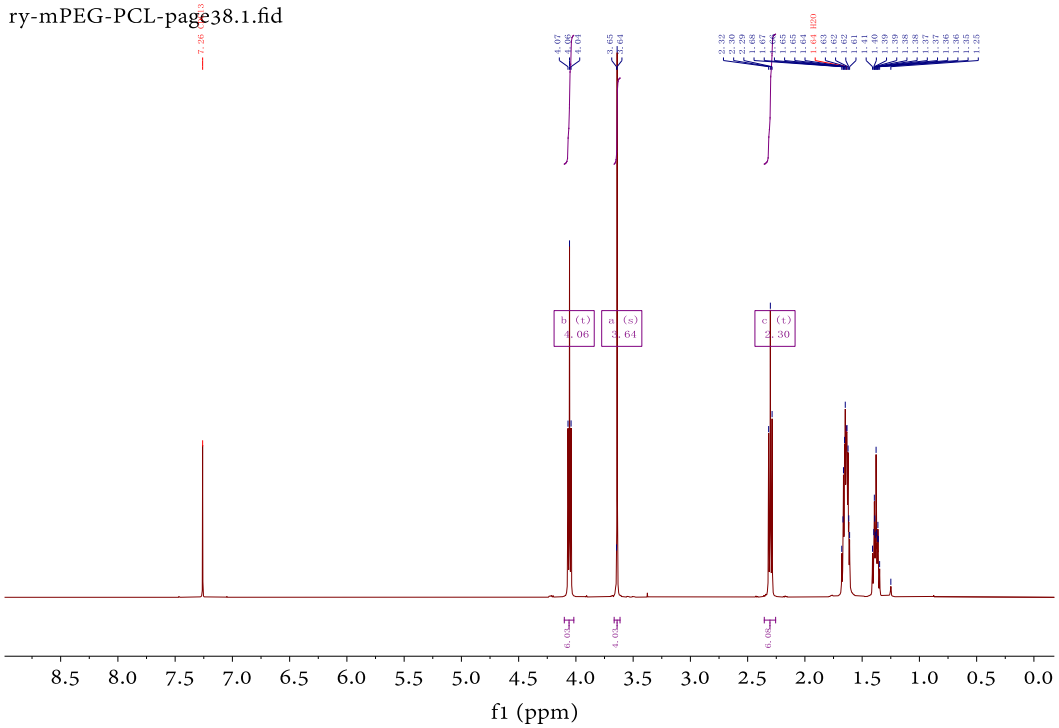

Figure 9 – Representative ^{1}H NMR Spectra, PCL-PEG$_{6k}$-PCL (above) and mPEG$_{5k}$-PCL (below).

2.4.3.2 Representative GPC Plot

GPC spectra were obtained using a GPC machine from Tosoh EcoSEC company (HLC 8320GPC model, TSKgel SuperHZ-L columns, PStQuick Mp-M polystyrene standards, eluting chloroform containing 0.25% triethylamine, flow rate of 0.45 mL/min, using). The MWs and Đs were then calculated based on refractive index chromatograms.

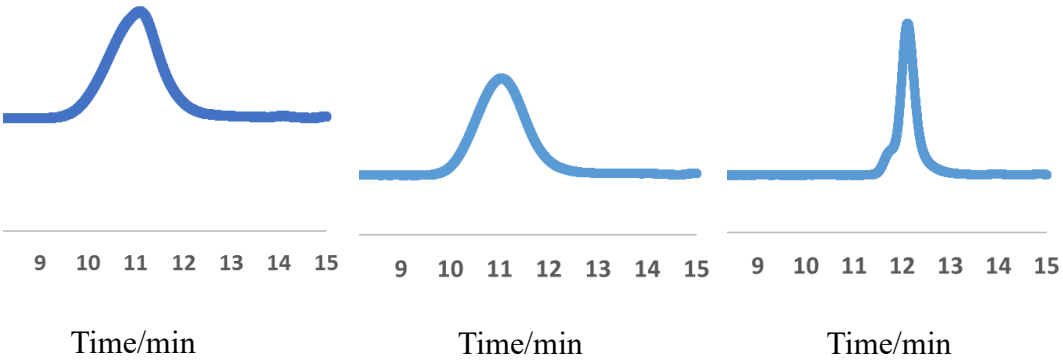

Figure 10 – Representative GPC Spectra of PCL (left, M_n = 50 kDa M_w = 85 kDa), mPEG$_{5k}$ (middle M_n = 10 kDa M_w = 12 kDa) and mPEG$_{5k}$-PCL (right M_n = 55 kDa M_w = 99 kDa).

2.4.3.3 Representative of TGA plot

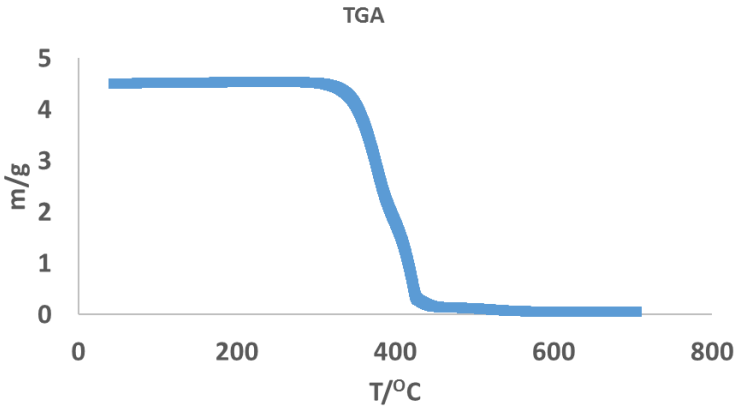

Figure 11 – Representative TGA Spectra of di-5k.

2.4.3.4 Representative of DSC plot

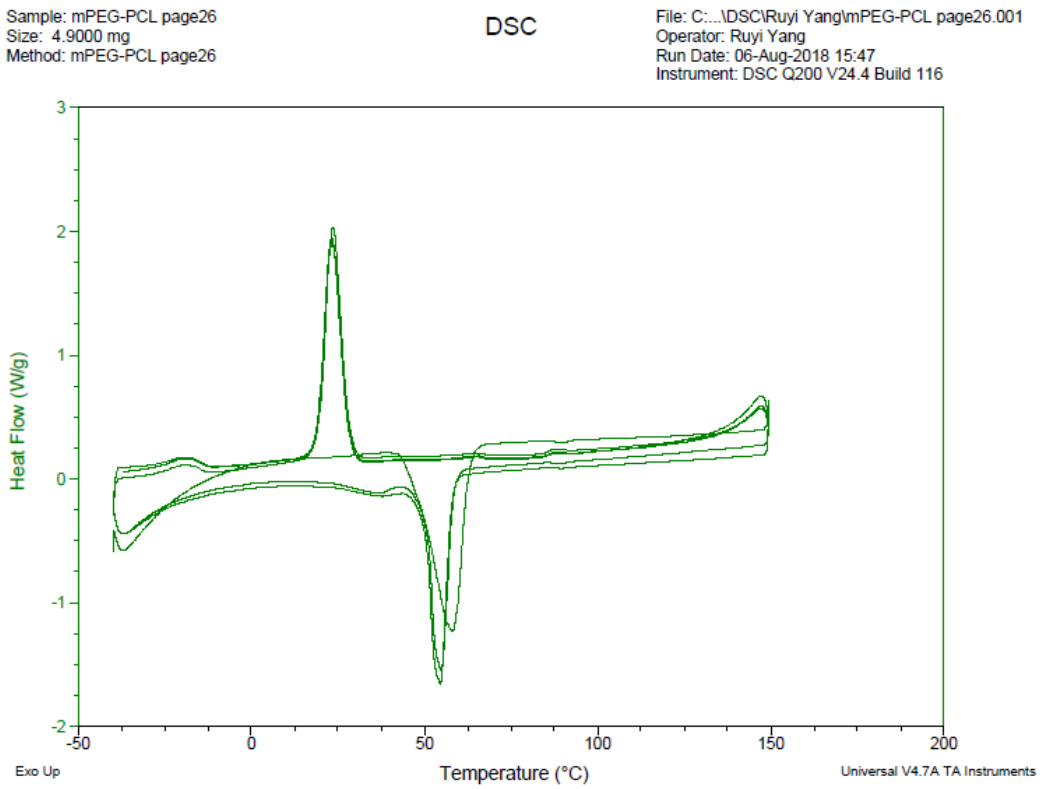

Figure 12 – Representative DSC Spectra of di-5k.

CHAPTER 3. APPLYING PEG-PCL POLYMERS FOR 3D PRINTING OF MEDICAL DEVICES

(Micro-CT data presented in this chapter were obtained from Adam Verga in Dr. Scott Hollister's lab at the Georgia Institute of Technology.)

3.1 Introduction

3.1.1 Airway reconstruction

An important clinical application of airway reconstruction is tracheobronchial malacia, which results in collapse of the airway during exhalation because of the reduced nonlinear elastic properties of primary airways.[46] The Hollister lab has previously studied the seriousness of this disease through computational models, showing that it can lead to respiratory arrest and subsequent death.[47] To solve this problem, patient-specific splints need to be fabricated based on the images from CT; hence, we hypothesized the use of 3D printing can create a difference in this area.

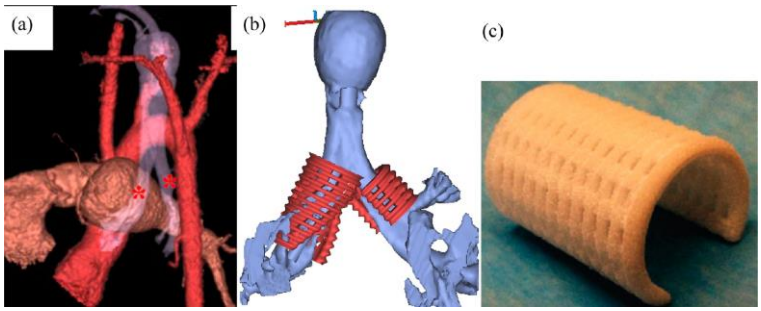

Figure 13 – Splint engineering process from patient image to 3D printed splint.[48]

Another clinical application of airway reconstruction we are interested in is laryngotracheoplasty to treat tracheal stenosis and laryngeal stenosis, which causes airway obstruction. Before open airway surgery was developed, endoscopic techniques (less popular nowadays) such as balloon dilation or sequential bougienage dilation was the main way to treat this disease. In contrast, open airway surgery shows favorable results. It consists of cricotracheal resection procedures, which cut off the narrow portion, and expansion procedures, that implant grafts to widen the airway, also known as laryngotracheoplasty. Although effective, resection faces more problems like possibility of damage to the laryngeal nerve, restenosis, anastomotic airway dehiscence, and technical challenges.[49]

As mentioned before, laryngotracheoplasty requires implantation of grafts. In such grafts, the most common and frequently used material is autologous cartilage, such as the one from thyroid, which is always used for anterior cricoid augmentation, costal and ear.[50, 51] However, donor site morbidity, long operative time to harvest, and the needs to carve the cartilage into patient-specific configuration are still unmet challenges.[52] As a consequence, various kinds of synthetic materials have been tested, such as LactoSorb, which is a copolymer of poly-L-lactic acid (PLLA, 82%) and polyglycolic acid (PGA, 18%).[53] In a rabbit model, this polymer showed desirable properties such as stability and integrity, but tests for stability inside larger animals needs further investigation. Synthetic materials also face challenges like complications related to infection, rejection, and scarring. In this thesis, we developed synthetic polymers based on FDA approved PCL device to address these challenges, potentially providing patient-specific graft by 3D printing, while preventing infection by introducing antimicrobial function to such synthetic polymers.

3.1.2 Craniofacial soft tissue engineering

Because of tumour resection, trauma or congenital defects, some patients lose or never grow some parts of tissues or organs. Tissue engineering offers the possibility to regenerate these tissues or organs. In facial plastic surgery, nasal and auricular reconstruction remain among the most challenging procedures. Based on specific design of patients' images from CT or MRI, commercial PCL has been widely used for the reconstruction. However, as a scaffold to support mammalian cells, PCL is too hydrophobic to adhere to them, which inhibits subsequent cell proliferation. Additionally, the high strength and modulus of PCL render it too rigid in many cases to design proper porous structures to serve soft tissue reconstruction. Moreover, post-implantation infections lead to serious problems, even death.[39, 54] My work introduces hydrophilic PEG block(s) to PCL that facilitates easier mammalian cell attachment and may improve cell proliferation. Also, the introduction of amorphous PEG block(s) will likely give rise to materials with lower modulus and strength, providing more compliant materials that are more ideal for soft tissue engineering. Moreover, a beneficial side-effect of PEG blocks is its ability to repel bacteria, potentially preventing implantation-related infections. These properties promise them great potential for the reconstruction of craniofacial soft tissue. In this chapter, we test several properties for the synthesized PCL-PEG block copolymers for their suitability as printable biomaterials.

3.2 Results

3.2.1 Porosity discrepancy and volume discrepancy

The effectiveness of a printing method is determined by comparing porosity and volume discrepancies of printed structures to the computer-aided design models. I used the extrusion method for printing with a 3D-Bioplotter Manufacturer Series from EnvisionTEC company. It uses heat to melt the materials for printing inside nozzles and then uses pneumatic pressure to print the 3D structures layer by layer with precise control.

As models for applications in laryngotracheoplasty, we designed two "table" shaped structures, one large and one small. To investigate the printing effectiveness for different materials, the large table structures were printed with pure PCL, tri-2k, and tri-6k materials (n=3). Small structures were printed with PCL, tri-6k, and di-10k (n=3). Each structure was scanned by micro-CT and the results are reported in Table 4 as percent void volume and percent volume error, respectively.

Table 4 – Porosity and volume discrepancies.

Group	Percent void volume	Percent volume error
All structures (n=18)	0.3355% ± 0.1615%	21.86% ± 5.35%
Large structures (n=9)	0.3164% ± 0.1815%	20.97% ± 4.14%
Small structures (n=9)	0.3546% ± 0.1472%	22.75% ± 6.48%
PCL-large (n=3)	0.2703% ± 0.0662%	17.32% ± 0.97%
Tri-2k-large (n=3)	0.3309% ± 0.3422%	21.72% ± 1.92%
Tri-6k-large (n=3)	0.3480% ± 0.0724%	23.87% ± 5.51%
PCL-small (n=3)	0.2322% ± 0.0333%	17.25% ± 1.27%
Tri-6k-small (n=3)	0.4741% ± 0.1151%	23.46% ± 0.70%
Di-10k-small (n=3)	0.3576% ± 0.1686%	27.55% ± 9.22%

When comparing all six groups to each other utilizing a one-way ANOVA test, no significant differences in porosity were evident ($p = 0.6088$, $n = 3$), and no significant differences in porosity were found when comparing any two of these six groups. When

comparing all small “table” structures to all large “table” structures using a t test, it was found that design did not have a significant effect on porosity ($p = 0.6313$, $n = 9$). When comparing only the three large groups by one-way ANOVA, the material was found not to have a significant effect on porosity ($p = 0.8904$, $n = 3$), and no significant differences in porosity were found when comparing any two of these three groups. Similarly, when comparing only the three small groups using a one-way ANOVA test, the nature of the material was again found not to have a significant effect on porosity ($p = 0.1202$, $n = 3$), and no significant differences in porosity were found when comparing any two of these three groups. However, when comparing the two materials which were printed using both large and small designs (PCL and PCL-PEG_{6k}-PCL), using a two-way ANOVA test with Tukey correction, the material did have a significant effect on porosity ($p = 0.0073$, $n = 3$) which emerged for the small “table” design prints ($p = 0.0211$, $n = 3$), but not the large “table” design ($p = 0.3536$, $n = 3$).

Similarly, for volume discrepancies, no significant differences were found between (a) all six groups to each other (one-way ANOVA, $p = 0.1009$, $n = 3$) or comparing any two groups, (b) small vs. large design groups (t test, $p = 0.6428$, $n = 9$), (c) comparing only the three large “table” groups (one-way ANOVA, $p = 0.1339$, $n = 3$) or any two of these groups, (d) comparing only the three small “table” groups (one-way ANOVA, $p = 0.1397$, $n = 3$) or any two of these groups, and (e) between large and small designs using the two materials which were used for both (two-way ANOVA with Tukey correction, $p = 0.8886$, $n = 3$). The only statistically significant difference in volume discrepancy was found for large vs. small designs for PCL and PCL-PEG_{6k}-PCL (two-way ANOVA with Tukey correction, $p = 0.0051$, $n = 3$).

The porosity of the printed samples, as evaluated using micro-CT, was consistently below one percent, as is expected from extrusion printing, since the high heat, long waiting period and pressure removes voids within the melt prior to deposition. Micro-CT also allowed for print path and surface morphology to be observed, and some surface defects were observed which were either from imprecise printing or handling and testing (Figure 14). As a result, the reported values are those of bulk porosity with surfaces excluded. Since only bulk porosity was considered, we did not expect this property to be significantly affected by minor design changes, which was confirmed by the results. Material composition was also found to not be significant for porosity when evaluated using one-way ANOVA tests between groups of the same design. This was also expected due to the similarities in composition, structure, and processing of the various materials used. Notably, a two-way ANOVA comparison between only PCL and PCL-PEG_{6k}-PCL did reveal a significant effect of the material but not of design. Therefore, while neither factor had a significant effect when considering this particular data set in its totality, material may show itself to be a more impactful factor than design in more extensive future studies. One reason for this may be thermomechanical property variations as a result of material composition, and processing parameters, which may affect uniformity and viscosities, leading to variations in printing behavior.

The volume discrepancy of extruded samples, as evaluated using micro-CT, was consistently above fifteen percent, as can be expected from extrusion printing, as a result of the fixed and relatively larger size of the extrusion line, as well as the imprecise nature of many extrusion systems. Print errors contributed to defects such as wavy extrusion lines, when they were intended to be straight, resulting in excess material volume being extruded.

Volume discrepancy analysis notably showed similar results to those of porosity analysis, although no correlation was found, with the effect of material composition seen when comparing PCL and PCL-PEG_{6k}-PCL being the only significant difference found in both volume discrepancy and porosity analyses. The significance of material in volume discrepancy as seen in this comparison could be due to the same factors which may affect porosity, for example the viscosity of the polymer melt.

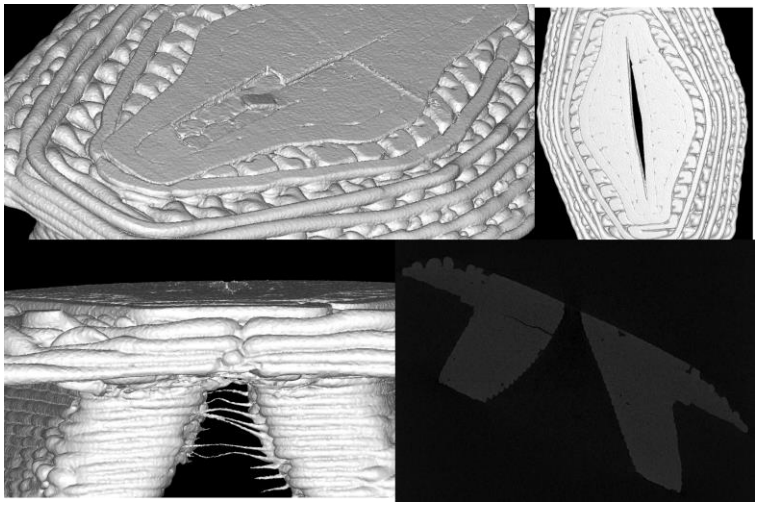

Figure 14 – Some examples of surface defects.

3.2.2 Bacterial adhesion test

To explore the bacterial adhesion-resistance properties of the products, Escherichia coli (*E. coli*) (DH5α, gram-negative) was chosen as a test case. Printing and sterilizing porous cylinders (around 50 % porosity) were followed by incubation inside bacterial suspensions. However, the di-20k and tri-20k groups swelled dramatically after a short

time in the bacterial suspensions, which substantially increased the surface area and caused much more bacteria attached (Figure 15).

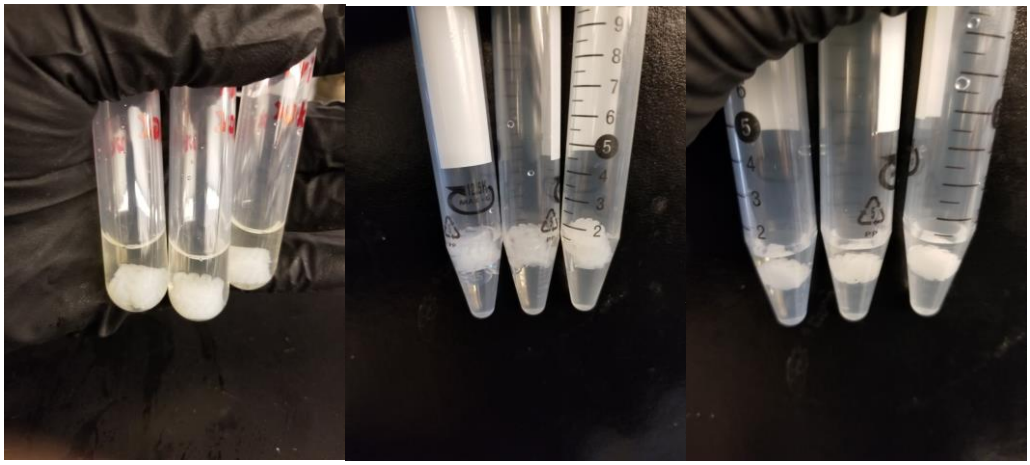

Figure 15 – The swelled porous structures of tri-20k group (left), di-20k group (middle) and normal-sized di-2k group (right).

For the other groups, after overnight shaking incubation at 37 ˚C, the bacterial suspensions were analysed by optical density (OD) measurement at 600 nm. The results were consistent, showing PCL and PEG-PCL materials to have no significant effect on bacterial replication, meaning that these materials were not bactericidal and similar amounts of bacteria had the possibility to adhere to the devices in each case.

To assess bacterial adhesion, the printed materials were withdrawn from the cell suspensions after overnight incubation, washed in PBS buffer to remove non- and weakly-adhered cells, and then sonicated individually in 1 mL PBS buffer. Aliquots of the resulting solutions were then cultured on agar plates and the bacterial colonies numbers were counted (Figure 16 and Figure 17). Comparisons between PCL (control) and PEG-PCL (experimental) groups were made using the Levene test for unequal variance, resulting in an overall p value of 0.0044, suggesting the need for the following nonparametric tests.

When comparing all PEG-PCL groups to PCL groups (Welch's one-way ANOVA), the di-5k, tri-6k, and tri-10k groups showed significantly fewer adhered live bacteria (p values of 0.0343, 0.0260, and 0.0019, respectively). This result supports our hypothesis that the introduction of PEG leads to materials that bind bacteria less well. While the failure of the di-2k and tri-2k polymers to resist bacterial adhesion is understandable (they have very little PEG in their formulations), the reason for the difference in performance between the triblock 10k (highly effective) and diblock 10k (not effective) materials is not apparent.

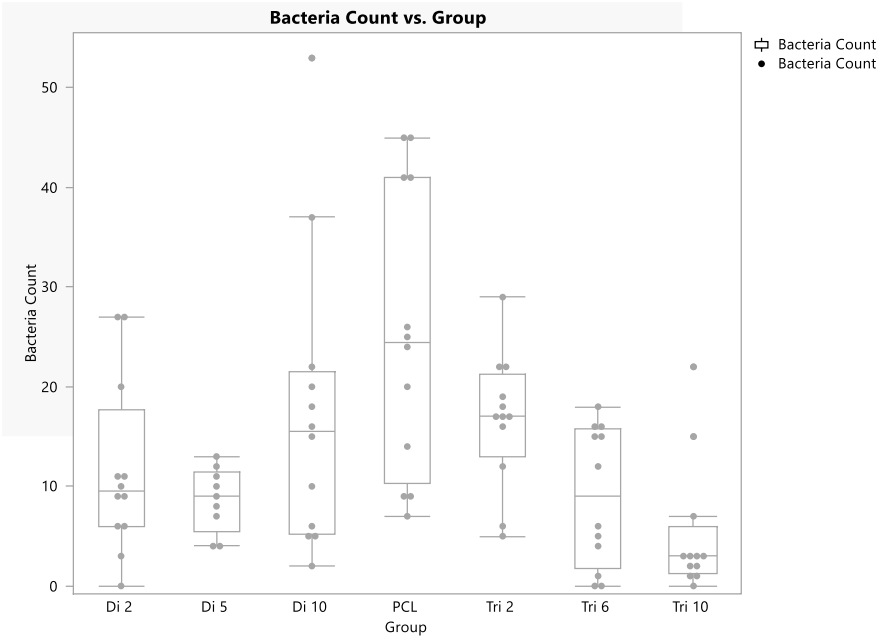

Figure 16 – Bacteria count vs. different groups.

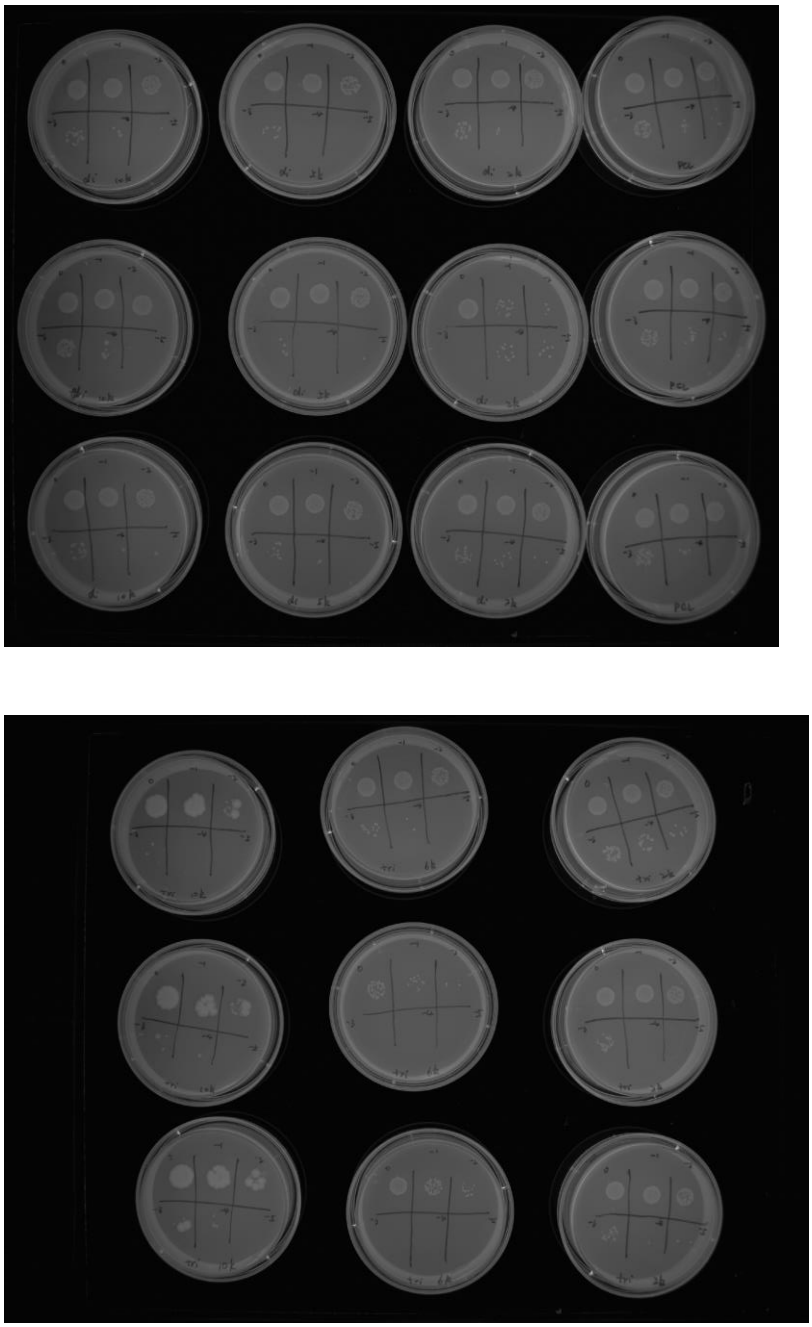

Figure 17 – Bacteria colonies on agar plates.

3.2.3 Mammalian cell attachment test

To explore the ability of the scaffolds to support mammalian cells, a common fibroblast cell line (NIH/3T3) was chosen for developing the cell attachment protocol. Circular polymer films (100 μm thick, 9 mm diameter) were printed to fit the wells in a 48 well plate. Each well was seeded with 0.2 million cells, the wells containing PCL, PEG-PCL, or no polymer as a control. Again, the tri-20k materials absorbed too much water and rapidly swelled so much that they could not be used (Figure 18). However, the di-20k materials swelled to a lesser degree and were still able to be anchored to the bottom surface of the wells with the help of O-rings. After incubating those wells for 18 h in Dulbecco's modified Eagle's Medium (DMEM) at 37 ˚C with 5 % carbon dioxide, the experimental films were washed with PBS three times to dislodge non-attached cells and further examined by alamar blue (AB) assay to quantitate the relative number of polymer-attached cells (Figure 19).

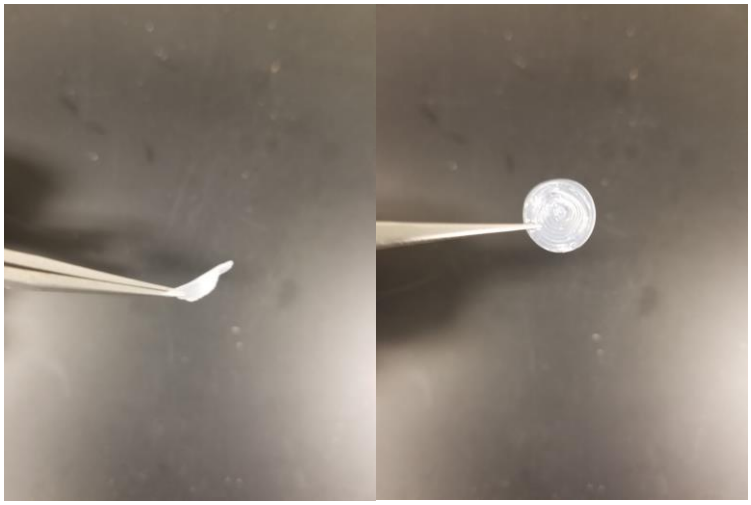

Figure 18 – The swelled tri-20k films.

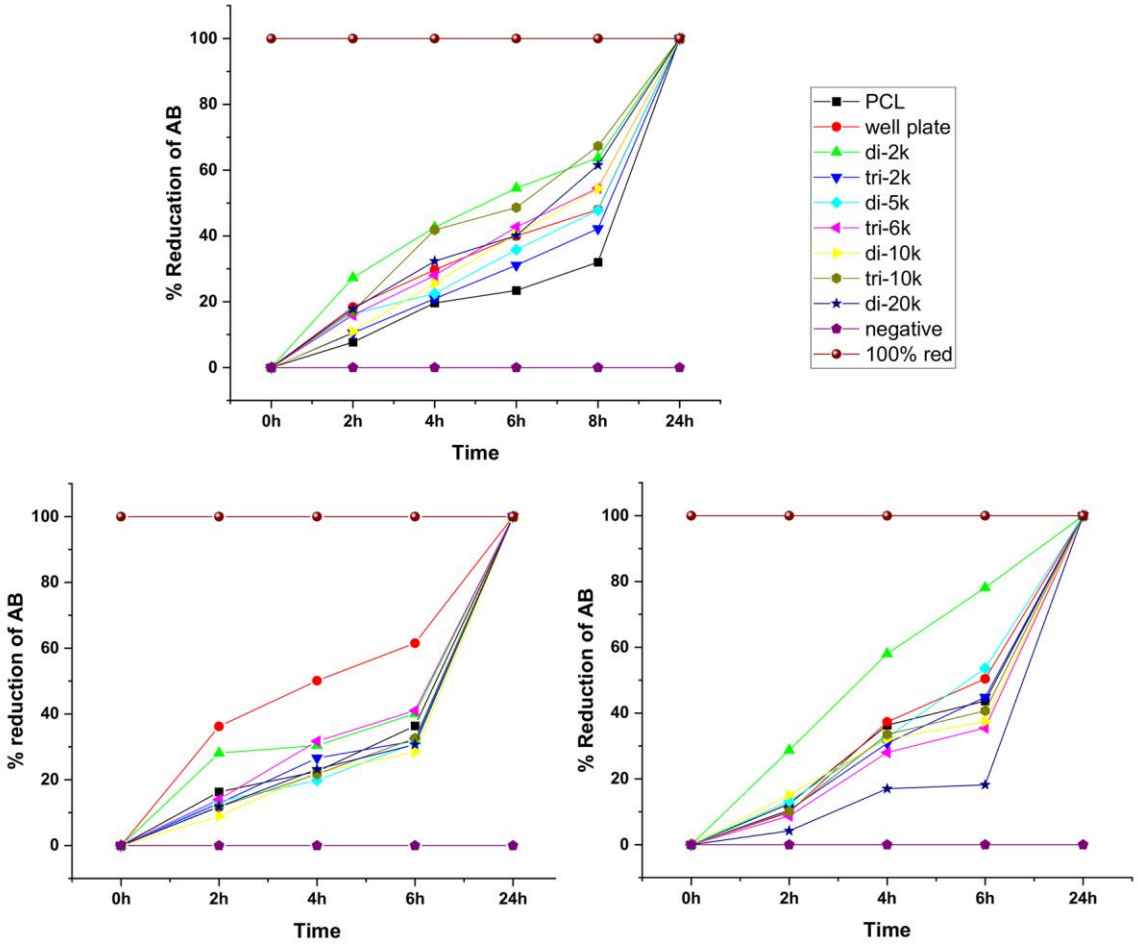

Figure 19 – Three repeat experiments for percentage of reduction of AB vs. time. Greater reduction in AB indicates more viable cells.

As shown in Figure 19, most of the block copolymer materials were similar to PCL for mammalian cell adhesion. However, we can see that di-2k had much more mammalian cell attachment with repeatable and reproducible results. Comparably, tri-2k and di-5k groups showed slightly better than PCL control group, with the others being similar to control group. This result is reasonable that the introduction of PEG can increase the hydrophilicity that the cells may have a better chance to attach to the surface. However, too much hydrophilicity will fully cover the surface with water molecules to avoid cells to

adhere. Based on these two factors, PEG with short to medium MW (di-2k, tri-2k and di-5k) showed relatively better results than pure PCL.

3.2.4 Mechanical properties

In addition to their interaction properties with cells, the mechanical properties of implanted medical devices are very important. We measured the stress-strain curves of standard printed shapes as described in the experimental section below. The compression Young's modulus and Poisson's ratio were obtained from these data by finite element analysis software with good quality fitting ($R^2 > 0.97$). These parameters were part of a Neo-Hookean viscoelastic fit to stress relaxation data. Meanwhile, the standard structures for three point bending test were also printed and tested, and flexure modulus was then calculated. Since the di-20k and tri-20k materials swelled a great deal, which is not desirable for the application, these were not examined.

The results, summarized in Figures 20 and 21, showed a range of modulus and Poisson's ratios, which can be used to give further directions for designing patterns of scaffolds to reach desired mechanical properties based on the different applications.

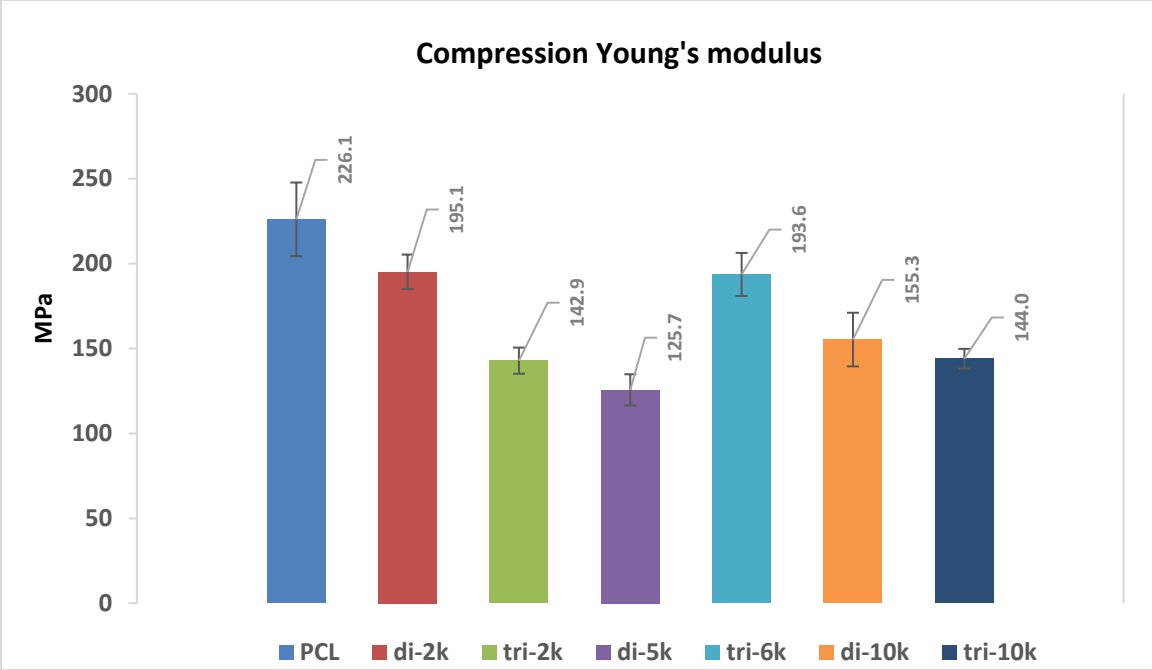

Figure 20 – Compression Young's modulus.

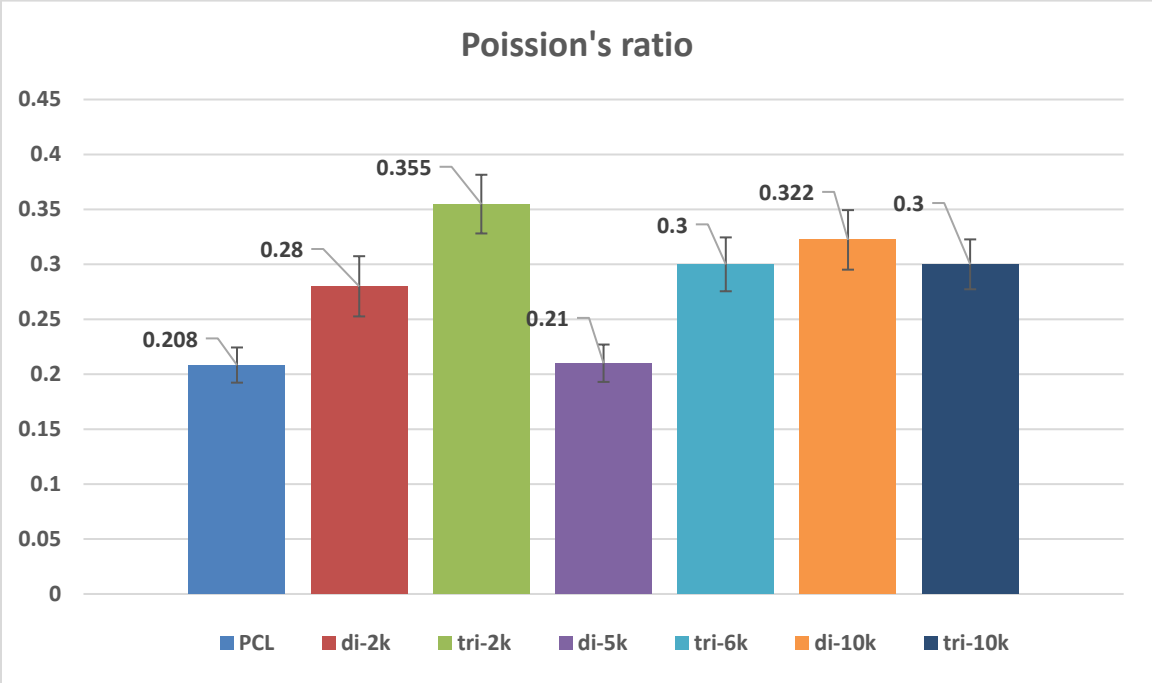

Figure 21 – Poisson's ratio.

To investigate the influence of pattern to the flexure modulus, two different patterns were designed and printed using the mPEG$_{5k}$-PCL material (Figure 22). The results showed that the patterns didn't influence the flexure modulus a lot, with the upper pattern having 739.7 ±55.7 MPa and the lower pattern having774.7±19.7 MPa. As a result, all materials were printed with the lower pattern.

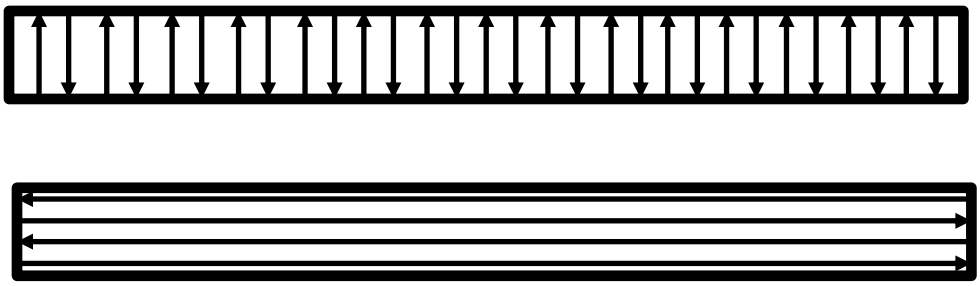

Figure 22 – Two different patterns for 3-point bending test structures.

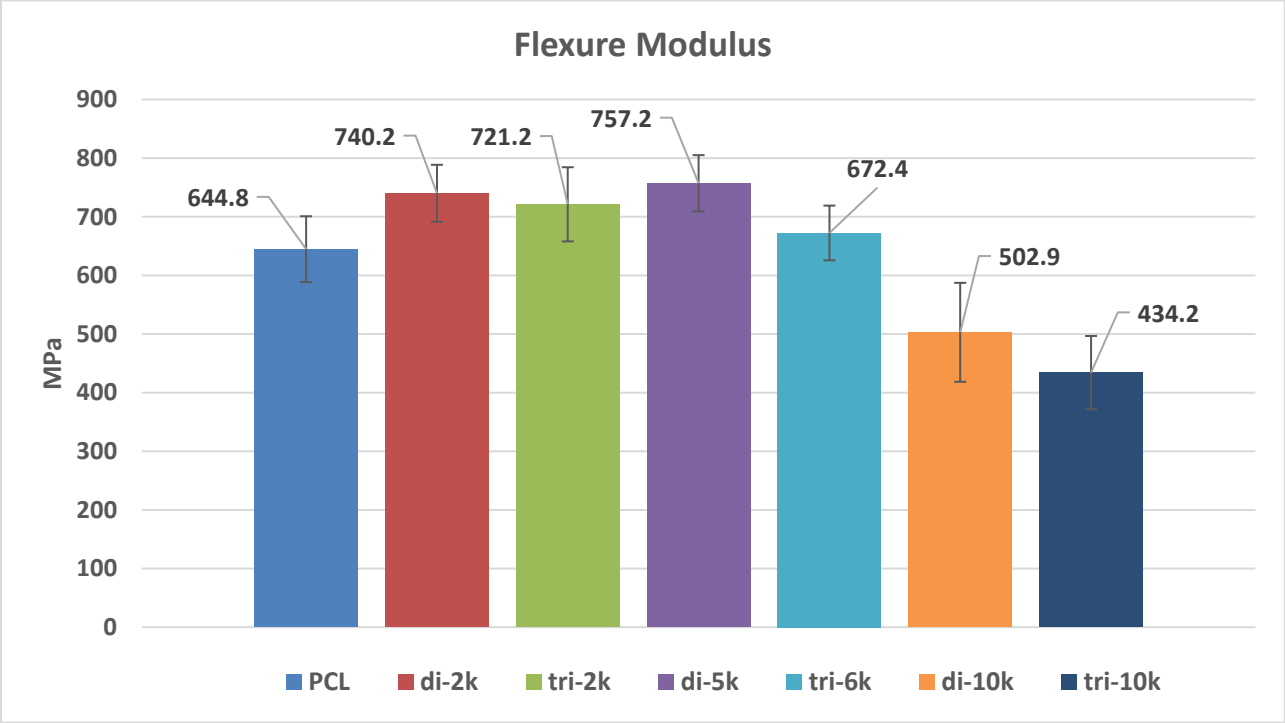

Figure 23 – Flexure Modulus.

The results, shown in Figure 23, indicated that the PEG-PCL polymers have good flexibility as pure PCL, which can afford the force during and after implantation, so that they are compatible for the application of biomedical devices. Also, these results can be used as given data when designing and estimating the flexibility of scaffolds using some software, such as SOLIDWORKS.

3.3 Conclusion

In this chapter, our objective was to test the properties of previously synthesized PEG-PCL block copolymers for applications in 3D printing of medical devices. As these copolymers are still new in the field of biomedical engineering, we started with early-stage experiments to explore their utility in such applications. Porosity discrepancy and volume discrepancy for some synthesized block copolymers were determined, and we found that the extrusion process was effective, and these materials were compatible with this printing method. Through bacterial assays, we determined that all PEG-PCL block copolymers, both diblock and triblock, were more effective than pure PCL in repelling bacteria. Notably, $mPEG_{5k}$-PCL diblock copolymer showed around 60% decreased bacterial cell attachment than pure PCL control. The best performer, triblock PCL-PEG_{10k}-PCL, repelled over 90% of bacteria compared to the control. In mammalian cell attachment experiments, we observed variability in each iteration since mammalian cells are more sensitive than bacterial cells. However, some polymers like di-2k, tri-2k, and di-5k often outperformed pure PCL. We evaluated the mechanical properties for each material, except di-20k and tri-20k, as potential implants go through different amounts of forces, since they are easily

breakable and swell a big ratio inside water-based solution, thereby limiting their application as medical devices. However, all other polymers showed great mechanical properties, which can be further tuned by designing different patterns, to be used for airway reconstruction and soft tissue engineering. Our data shows promising results for applications of PEG-PCL block copolymer materials as 3D printable medical devices.

3.4 Experimental

3.4.1 Micro-CT

Microcomputed tomography (micro-CT) was conducted using a uCT50 (SCANCO Medical AG, Bruttisellen, Switzerland). Samples (n=3) were placed into a 19mm sample holder, which possesses a 20.5mm field of view, and scanned with 55kVp, 145uA and 200ms integration time, resulting in a 20um voxel size. Analysis, evaluating bulk percent void volume, was conducted using Mimics v23.0 (Materialise NV, Leuven, Belgium). At least 100um inward from the surface was ignored when recording porosity data to avoid artifacts from surface defects. Porosity, reported as percent void volume, was calculated using equation (1), and volume discrepancy, reported as percent volume error, was calculated using equation (2).

1. Percent void volume = 100 * (eroded filled volume – eroded unfilled volume) / eroded filled volume
2. Volume discrepancy = 100 * abs (design volume – total unfilled volume) / design volume

Statistical analysis on micro-CT data was conducted using Prism v9.2.0 (GraphPad Software, San Diego CA, USA). One-way and two-way ANOVA tests as well as unpaired two-tailed t tests were used depending on the data being compared, with Tukey correction used for multiple comparisons tests.

3.4.2 Mechanical Properties Test

To serve as ideal scaffolds, the printed polymers should have enough mechanical strength to support the cells, retain their shape, withstand *in vivo* force, and allow surgical handling during implantation. Finite element analysis software is the method we used to estimate the compressive Young's modulus and Poisson's ratio of a design structure from stress-relaxation tests, which could help to avoid numerous experiments and thus accelerate the paces of design refinement. To get the accurate estimation, compression tests were done before stress-relaxation tests and fitting. According to ASTM D695 standards, cylinders with a 5 mm diameter, a 10 mm height were printed (n=5 for each material) with 3D BIOPLOTTER for compression tests by an Instron device (Model: 5944). In stress-strain plots, the slope of linear part is the Young's modulus and move the tangent line to the right for 0.2% to get the intersection, which is the offset strength. The plot gave the range of compression displacement in future stress-relaxation tests, and the calculated modulus served as the initial estimation range for fitting.

Meanwhile, specimens with a 50 mm length, a 5 mm width and a 2 mm height were printed for three-point bending tests (n=5 for each sample) and tested using Instron device (Model: 5944). The flexural modulus (E_f) (MPa) were calculated by equation below, where

L (mm) is the distance between two supporting points (in this case, 30 mm), m (N/mm) is the slope of the initial straight-line portion of the load deflection curve, b (mm) and d (mm) are the width and depth of the test specimens.

$$E_f = \frac{L^3 m}{4bd^3}$$

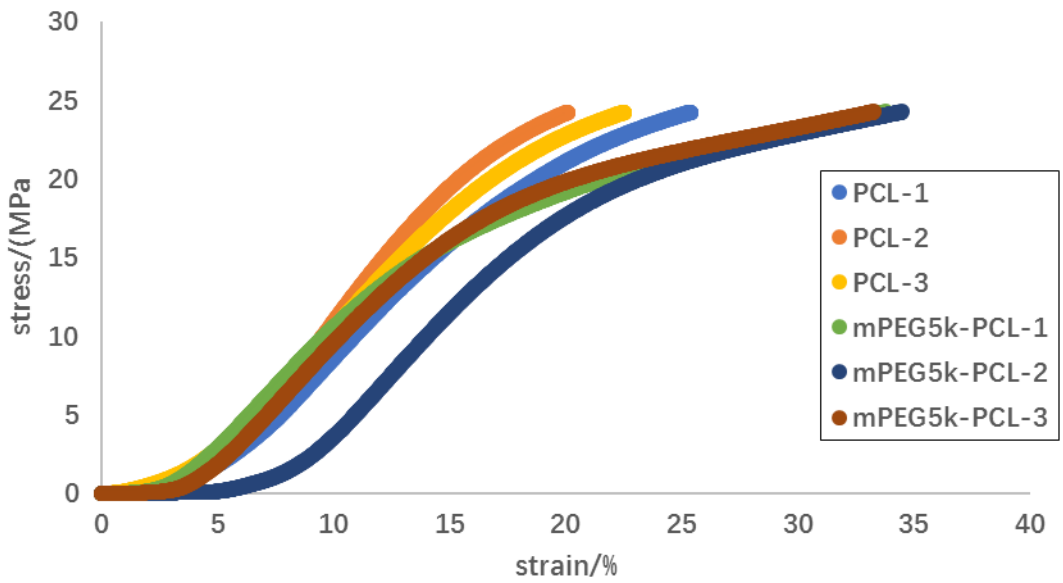

Figure 24 – An example of stress-strain plots for PCL and mPEG$_{5k}$-PCL.

3.4.3 Bacterial Adhesion Test

To explore the bacterial adhesion-resistance properties of the products, *Escherichia coli* (*E. coli)* (DH5α, gram-negative) was chosen as a test case for developing the bacterial adhesion protocol. The assay workflow is shown in Figure 25. Printing and sterilizing porous cylinders (around 50 % porosity) were followed by incubation inside 2 mL bacterial suspension (in Mueller-Hinton Broth (MHB) medium) with total amount of colony-forming units (CFU) of 0.06. After overnight shaking incubation, the bacterial suspensions

were analyzed by optical density (OD) measurement at 600 nm. The consistent results from PCL control group, PEG-PCL experiment groups, negative control (bacteria alone) group indicated that these materials were not cytotoxic and similar amounts of bacteria had the possibility to adhere to the devices. The non-adherent bacteria at the surface of the devices were removed by washing in phosphate-buffered saline (PBS) three times, and the adhered bacteria were collected by sonication and then vortex mixing in 1 mL PBS three times. The resulting liquid was analyzed on agar spot plates with five serial dilutions from 10^0 to 10^{-5}, and incubated at 37 °C overnight. The bacterial colonies numbers were counted and compared between PCL and PEG-PCL experimental groups.

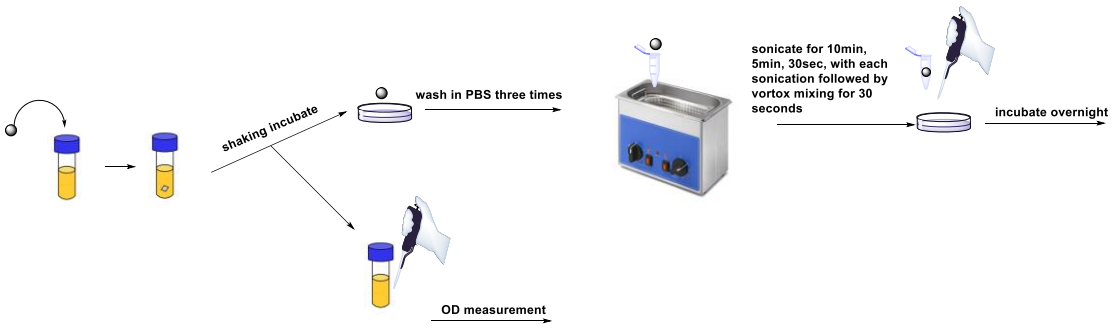

Figure 25 – Bacterial adhesion assay.

3.4.4 Mammalian Cell Attachment Test

To explore the ability of the scaffolds to support the cells, NIH/3T3 cells, a common fibroblast cell line, was chosen for developing the cell attachment protocol. The assay workflow is shown in Figure 26. Circular polymer films with a 100 μm thickness and a 9 mm diameter were printed to fit the wells in a 48 well plate. Silicone O-rings were used to avoid floating of the films. To increase the possibility of cell attachment, experimental and control groups were cultured in 0.7 mL Dulbecco's modified Eagle's Medium (DMEM)

containing 5% fetal bovine serum (FBS) under standard conditions of 5% CO_2 in air at 37 °C overnight. After that, 0.05 million cells were seeded to PCL, PEG-PCL experimental groups, one positive control group (well surface), meanwhile medium instead of cell suspension being added to negative control group, and cultured for 20 h. Then they were washed with PBS to dislodge non-attached cells, and examined by alamar blue (AB) assay to quantitate the relative number of polymer-attached cells. The adhered cells were incubated with 10% v/v alamar blue regents in 0.4 mL phenol red free DMEM medium containing 1% FBS for a series of time points to explore the proper incubation time. The AB regents were quantitively reduced to fluorescent products according to the number of cells. The fluorescence signal of reduced alamar blue regents was detected by a plate reader with an excitation wavelength of 560 nm and an emission wavelength of 590 nm and the reduction of AB then was calculated with the equation below. The 100% reduced positive control relative fluorescence units (RFU) value was gained by adding 1.5 mg (10 μL) vitamin C to AB per well. The negative control RFU value was gained by detecting the fluorescence signal from 10% v/v alamar blue regents in 0.4 mL phenol red free DMEM medium containing 1% FBS without any cells.

$$\%\ \text{Reduction of AB} = \frac{\text{Experimental RFU value} - \text{Negative control RFU value}}{\text{100\% Reduced positive control RFU value} - \text{Negative control RFU value}} \times 100$$

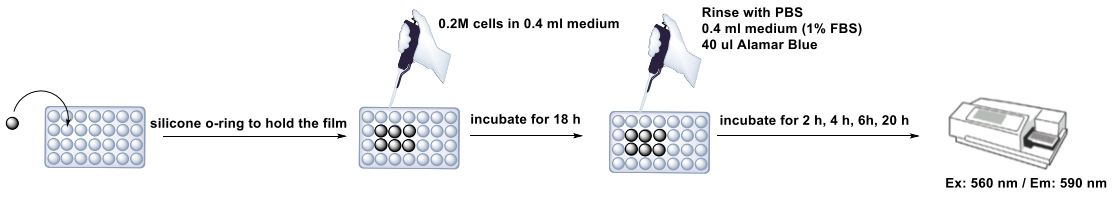

Figure 26– Mammalian cell attachment assay.

CHAPTER 4. CONCLUSION AND OUTLOOK

4.1 Concluding Remarks

My overall aim in this dissertation was to modify a standard PCL polymer to be more suitable for use in medical devices while retaining the ability to be 3D printed. The inclusion of a PEG block was a conceptually simple idea, but surprisingly had not been well explored in the literature. Both PEG and PCL polymers are well established for their biological applications. PEG-PCL copolymers have also been reported to be suitable for 3D printing and non-cytotoxic to mammalian cells. However, to the best of our knowledge, a comprehensive study of three important parameters—printability, mammalian cell attachment, and bacterial repulsion—for different ratios of PEG:PCL within the same overall molecular weight was missing.

I therefore synthesized several types of polymers with differing PEG to PCL ratios in polymers of approximately 43 kDa total molecular weight. These syntheses were performed on sufficient scale for the 3D printing of a variety of test samples. In Chapter 2, we showed that all the synthesized polymers can be 3D printed by the extrusion process using a 3D BIOPLOTTER instrument, adjusting the printing parameters to accommodate changes in viscosity, melting temperature, and degradation temperature. In Chapter 3, we assessed bacterial cell attachment to each of these polymers. The di-5k, tri-6k and tri-10k groups showed significantly more resistance to bacterial adhesion compared to commercial PCL. For the application of tissue engineering, it is important to avoid bacteria, but attach mammalian cells. Hence, we also tested fibroblast NIH/3T3 cell attachment with our polymers, and among them di-2k, tri-2k, di-5k showed good results. Also, these polymers

showed excellent mechanical properties, which can be further modified by printing with different patterns. In all, for the application of airway reconstruction, di-5k, tri-6k and tri-10k are the best candidates; for the application of craniofacial soft tissue application, di-5k is preferred as it can attach mammalian cells and repel bacterial cells at the same time.

Overall, this years-long study aimed to create and identify the best PEG/PCL ratio for 3D printing of medical devices for two medical applications. The chapter breakdown in this thesis correlates to the workflow: find suitable materials, synthesize them, test their potential as medical implants, and find ways to improve them.

4.2 Future Directions

It is known that PEG repels a significant percentage of bacteria, however, it is not 100% effective. Our immediate steps are to find ways to repel most of bacteria and kill the ones remaining, since bacterial attachment or growth is not ideal for implantations. Another common bacteria-repel material is zwitterionic groups on the polymeric backbone, which can be also tried and explored their influence on mammalian cells. To kill the bacteria, biocides can be incorporated into the polymer, for example, thiabicyclononane-based materials developed in our lab before. We can do this by using a functionalized PCL monomer like chloro-caprolactone and copolymerize with PEG. The chlorine groups can be further substituted by azide groups post-polymerization and then clicked to any such zwitterionic or polycationic groups post-printing. Apart from tests for fibroblast attachment with the polymer, we can also test for the proliferation of these cells. Additionally, these

materials can then be tested—both in vivo and in vitro—for their degradation time and tissue generation.

REFERENCES

1. Bekas, D. G.; Hou, Y.; Liu, Y.; Panesar, A., 3D printing to enable multifunctionality in polymer-based composites: A review. *Composites Part B: Engineering* **2019,** *179*.

2. Xu, W.; Jambhulkar, S.; Zhu, Y.; Ravichandran, D.; Kakarla, M.; Vernon, B.; Lott, D. G.; Cornella, J. L.; Shefi, O.; Miquelard-Garnier, G.; Yang, Y.; Song, K., 3D printing for polymer/particle-based processing: A review. *Composites Part B: Engineering* **2021,** *223*.

3. Zak C. Eckel, C. Z., John H. Martin, Alan J. Jacobsen,William B. Carter, Tobias A. Schaedler, Additive manufacturing ofpolymer-derived ceramics. *Science* **2016,** *351* (6268).

4. Park, J. H.; Jang, J.; Lee, J. S.; Cho, D. W., Three-Dimensional Printing of Tissue/Organ Analogues Containing Living Cells. *Ann Biomed Eng* **2017,** *45* (1), 180-194.

5. Tian, Y.; Chen, C.; Xu, X.; Wang, J.; Hou, X.; Li, K.; Lu, X.; Shi, H.; Lee, E. S.; Jiang, H. B., A Review of 3D Printing in Dentistry: Technologies, Affecting Factors, and Applications. *Scanning* **2021,** *2021*, 9950131.

6. Soo, A.; Ali, S. M.; Shon, H. K., 3D printing for membrane desalination: Challenges and future prospects. *Desalination* **2021,** *520*.

7. Walia, K.; Khan, A.; Breedon, P., Polymer-Based Additive Manufacturing: Process Optimisation for Low-Cost Industrial Robotics Manufacture. *Polymers (Basel)* **2021,** *13* (16).

8. Hensleigh, R.; Cui, H.; Xu, Z.; Massman, J.; Yao, D.; Berrigan, J.; Zheng, X., Charge-programmed three-dimensional printing for multi-material electronic devices. *Nature Electronics* **2020,** *3* (4), 216-224.

9. Wallis, M.; Al-Dulimi, Z.; Tan, D. K.; Maniruzzaman, M.; Nokhodchi, A., 3D printing for enhanced drug delivery: current state-of-the-art and challenges. *Drug Dev Ind Pharm* **2020,** *46* (9), 1385-1401.

10. ASTM52900 - 15: Standard Terminology for Additive Manufacturing –

General Principles – Terminology. *ASTM International* **2015**.

11. Gibson, I. R., D.; Stucker, B. Binder Jetting, In Additive Manufacturing Technologies: 3D Printing, Rapid

Prototyping, and Direct Digital Manufacturing. *Springer* **2015**, 205-218.

12. Mirzababaei, S.; Pasebani, S., A Review on Binder Jet Additive Manufacturing of 316L Stainless Steel. *Journal of Manufacturing and Materials Processing* **2019,** *3* (3).

13. Dass, A.; Moridi, A., State of the Art in Directed Energy Deposition: From Additive Manufacturing to Materials Design. *Coatings* **2019,** *9* (7).

14. Lee, H.; Lim, C. H. J.; Low, M. J.; Tham, N.; Murukeshan, V. M.; Kim, Y.-J., Lasers in additive manufacturing: A review. *International Journal of Precision Engineering and Manufacturing-Green Technology* **2017,** *4* (3), 307-322.

15. Ngo, T. D.; Kashani, A.; Imbalzano, G.; Nguyen, K. T. Q.; Hui, D., Additive manufacturing (3D printing): A review of materials, methods, applications and challenges. *Composites Part B: Engineering* **2018,** *143*, 172-196.

16. Meena Panta, P. P., Harish Kumara, Leeladhar Nagdevea, Girija Moonab, Additive manufacturing: The significant role in biomedical and aerospace applications. *Indian Journal of Engineering & Materials Sciences* **2021,** *28*, 330-342.

17. Shilo, D.; Emodi, O.; Blanc, O.; Noy, D.; Rachmiel, A., Printing the Future-Updates in 3D Printing for Surgical Applications. *Rambam Maimonides Med J* **2018,** *9* (3).

18. Tejo-Otero, A.; Buj-Corral, I.; Fenollosa-Artes, F., 3D Printing in Medicine for Preoperative Surgical Planning: A Review. *Ann Biomed Eng* **2020,** *48* (2), 536-555.

19. Wang, Z.; Yang, Y., Application of 3D Printing in Implantable Medical Devices. *Biomed Res Int* **2021,** *2021*, 6653967.

20. Yan, Q.; Dong, H.; Su, J.; Han, J.; Song, B.; Wei, Q.; Shi, Y., A Review of 3D Printing Technology for Medical Applications. *Engineering* **2018,** *4* (5), 729-742.

21. Wu, G. H.; Hsu, S. H., Review: Polymeric-Based 3D Printing for Tissue Engineering. *J Med Biol Eng* **2015,** *35* (3), 285-292.

22. Dylan Jack Richards, Y. T., Jia Jia, Hai Yao, and Ying Mei, 3D Printing for Tissue Engineering. *Isr J Chem* **2013,** *53*.

23. Zopf, D. A.; Mitsak, A. G.; Flanagan, C. L.; Wheeler, M.; Green, G. E.; Hollister, S. J., Computer aided-designed, 3-dimensionally printed porous tissue bioscaffolds for craniofacial soft tissue reconstruction. *Otolaryngol Head Neck Surg* **2015,** *152* (1), 57-62.

24. Wu, D.; Yu, Y.; Tan, J.; Huang, L.; Luo, B.; Lu, L.; Zhou, C., 3D bioprinting of gellan gum and poly (ethylene glycol) diacrylate based hydrogels to produce human-scale constructs with high-fidelity. *Materials & Design* **2018,** *160*, 486-495.

25. Ding, S.; Feng, L.; Wu, J.; Zhu, F.; Tan, Z.; Yao, R., Bioprinting of Stem Cells: Interplay of Bioprinting Process, Bioinks, and Stem Cell Properties. *ACS Biomater Sci Eng* **2018,** *4* (9), 3108-3124.

26. Mehrban, N.; Teoh, G. Z.; Birchall, M. A., 3D bioprinting for tissue engineering: Stem cells in hydrogels. *International Journal of Bioprinting* **2016,** *2* (0).

27. O'Brien, F. J., Biomaterials & scaffolds for tissue engineering. *Materials Today* **2011,** *14* (3), 88-95.

28. Parak, A.; Pradeep, P.; du Toit, L. C.; Kumar, P.; Choonara, Y. E.; Pillay, V., Functionalizing bioinks for 3D bioprinting applications. *Drug Discov Today* **2019,** *24* (1), 198-205.

29. Bhatia, A.; Sehgal, A. K., Additive manufacturing materials, methods and applications: A review. *Materials Today: Proceedings* **2021**.

30. Zak C. Eckel, C. Z., John H. Martin, Alan J. Jacobsen,; William B. Carter, T. A. S., Additive manufacturing of polymer-derived ceramics. *Science* **2016,** *351* (6268).

31. Shalin Shaunak, B. S. D. a. W. S. K., The Role of 3D Modelling and Printing in Orthopaedic Tissue Engineering: A Review of the Current Literature. *Current Stem Cell Research & Therapy* **2017,** *12*.

32. Xu, T.; Binder, K. W.; Albanna, M. Z.; Dice, D.; Zhao, W.; Yoo, J. J.; Atala, A., Hybrid printing of mechanically and biologically improved constructs for cartilage tissue engineering applications. *Biofabrication* **2013,** *5* (1), 015001.

33. Wang, W.; Caetano, G.; Ambler, W. S.; Blaker, J. J.; Frade, M. A.; Mandal, P.; Diver, C.; Bartolo, P., Enhancing the Hydrophilicity and Cell Attachment of 3D Printed PCL/Graphene Scaffolds for Bone Tissue Engineering. *Materials (Basel)* **2016,** *9* (12).

34. Qian, Y.; Zhao, X.; Han, Q.; Chen, W.; Li, H.; Yuan, W., An integrated multi-layer 3D-fabrication of PDA/RGD coated graphene loaded PCL nanoscaffold for peripheral nerve restoration. *Nat Commun* **2018,** *9* (1), 323.

35. Altun, E., Ekren, Nazmi, Kuruca, Serap Erdem, Gunduz, Oguzhan, Cell studies on Electrohydrodynamic (EHD)-3D-bioprinted Bacterial Cellulose\Polycaprolactone scaffolds for tissue engineering. *Materials Letters* **2019,** *234*, 163-167.

36. Jiang, C. P.; Chen, Y. Y.; Hsieh, M. F., Biofabrication and in vitro study of hydroxyapatite/mPEG-PCL-mPEG scaffolds for bone tissue engineering using air pressure-aided deposition technology. *Mater Sci Eng C Mater Biol Appl* **2013,** *33* (2), 680-90.

37. Jiang, C. P.; Huang, J. R.; Hsieh, M. F., Fabrication of synthesized PCL-PEG-PCL tissue engineering scaffolds using an air pressure-aided deposition system. *Rapid Prototyping Journal* **2011,** *17* (4), 288-297.

38. Zhang, H.; Lin, C. Y.; Hollister, S. J., The interaction between bone marrow stromal cells and RGD-modified three-dimensional porous polycaprolactone scaffolds. *Biomaterials* **2009,** *30* (25), 4063-9.

39. Yu, Q.; Wu, Z.; Chen, H., Dual-function antibacterial surfaces for biomedical applications. *Acta Biomater* **2015,** *16*, 1-13.

40. Murata, H.; Koepsel, R. R.; Matyjaszewski, K.; Russell, A. J., Permanent, non-leaching antibacterial surface--2: how high density cationic surfaces kill bacterial cells. *Biomaterials* **2007,** *28* (32), 4870-9.

41. Geng, Z.; Finn, M. G., Thiabicyclononane-Based Antimicrobial Polycations. *J Am Chem Soc* **2017,** *139* (43), 15401-15406.

42. Robert G. Chapman, E. O., Michael N. Liang, Gloria Meluleni, Enoch Kim,§ Lin Yan,† Gerald Pier, H. Shaw Warren, and; Whitesides, G. M., Polymeric Thin Films That Resist the Adsorption of Proteins and the Adhesion of Bacteria. *Langmuir* **2001,** *17*, 1225-1233.

43. Cheng, G.; Zhang, Z.; Chen, S.; Bryers, J. D.; Jiang, S., Inhibition of bacterial adhesion and biofilm formation on zwitterionic surfaces. *Biomaterials* **2007,** *28* (29), 4192-9.

44. Francolini, I.; Silvestro, I.; Di Lisio, V.; Martinelli, A.; Piozzi, A., Synthesis, Characterization, and Bacterial Fouling-Resistance Properties of Polyethylene Glycol-Grafted Polyurethane Elastomers. *Int J Mol Sci* **2019,** *20* (4).

45. Neil P.Desai, S. F. A. H., Jeffrey A. Hubbell, Surface-immobilized polyethylene oxide for bacterial repellence *Biomaterials* **1992,** *13*.

46. Morrison, R. J.; Sengupta, S.; Flanangan, C. L.; Ohye, R. G.; Hollister, S. J.; Green, G. E., Treatment of Severe Acquired Tracheomalacia With a Patient-Specific, 3D-Printed, Permanent Tracheal Splint. *JAMA Otolaryngol Head Neck Surg* **2017,** *143* (5), 523-525.

47. Hollister, S. J.; Hollister, M. P.; Hollister, S. K., Computational modeling of airway instability and collapse in tracheomalacia. *Respir Res* **2017,** *18* (1), 62.

48. Hollister, S. J.; Flanagan, C. L.; Morrison, R. J.; Patel, J. J.; Wheeler, M. B.; Edwards, S. P.; Green, G. E., Integrating Image-Based Design and 3D Biomaterial Printing to create Patient Specific Devices within a Design Control Framework for Clinical Translation. *ACS Biomater Sci Eng* **2016,** *2* (10), 1827-1836.

49. Smith, M. M.; Cotton, R. T., Diagnosis and management of laryngotracheal stenosis. *Expert Rev Respir Med* **2018,** *12* (8), 709-717.

50. Gaffey, M. M.; Sun, R. W.; Richter, G. T., A novel surgical treatment for posterior glottic stenosis using thyroid ala cartilage - A case report and literature review. *Int J Pediatr Otorhinolaryngol* **2018,** *114*, 129-133.

51. Jang, M.; Grunstein, E., Endoscopic Posterior Cricoid Split and Rib Graft Without Tracheostomy: Case and Literature Review. *Laryngoscope* **2021,** *131* (9), E2599-E2602.

52. Peter J. Koltai, B. E., James Chan, Anthony Calabro, Anterior and Posterior Cartilage Graft Dimensions in Successful Laryngotracheal Reconstruction. *ARCH OTOLARYNGOL HEAD NECK SURG* **2006,** *132*.

53. Klein, A. M.; Graham, V. L.; Gulleth, Y.; Lafreniere, D., Polyglycolic acid/poly-L-lactic acid copolymer use in laryngotracheal reconstruction: a rabbit model. *Laryngoscope* **2005,** *115* (4), 583-7.

54. Desrousseaux, C.; Sautou, V.; Descamps, S.; Traore, O., Modification of the surfaces of medical devices to prevent microbial adhesion and biofilm formation. *J Hosp Infect* **2013,** *85* (2), 87-93.